PHOTOLUMINESCENCE SPECTROSCOPY OF SINGLE FREE STANDING QUANTUM WELLS

A THESIS

SUBMITTED TO THE FACULTY OF CLARK ATLANTA UNIVERSITY

IN PARTIAL FULFILLMENT OF THE REQUIREMENTS FOR

THE DEGREE OF MASTER OF SCIENCE

BY

ADWOA K. GYEKYE

DEPARTMENT OF PHYSICS

ATLANTA, GEORGIA

DECEMBER 2004

ABSTRACT

PHYSICS

GYEKYE, ADWOA KHADIJAH

PHOTOLUMINESCENCE SPECTROSCOPY OF SINGLE FREE STANDING QUANTUM WELLS

Advisor: Dr. Michael Williams

Thesis dated December 2004

Multilayer material systems, like quantum wells, are increasingly important in the development of smaller, faster, and more efficient electronic and optoelectronic devices. The scope of this project is twofold. It first involves the study and use of the photoluminescence spectroscopy surface characterization technique for nanoscale structures. Then the study of nanoscale gallium arsenide quantum well structures is done. The aim is to investigate the interaction of the quantum confined exciton states in free standing GaAs quantum wells with native and adsorbed surface states by using photoluminescence spectroscopy to probe the unique bare freestanding quantum wells structures. Single Molecule Photoluminescence, a sensitive methodology for detecting light from single molecules, is the process used. It offers the spatial resolution necessary to analyze the area of interest. There is also the added advantage of having the capability of studying adsorbate interactions which has important ramifications for sensor technology.

ACKNOWLEDGEMENTS

The author is especially grateful to Dr. Thomas Huser, of Lawrence Livermore National Laboratories, for his support and use of his laboratory facilities. Further thanks go to Anthony Esposito for assistance with data collection and providing many clarifying and useful materials. Many thanks go to Damian Cupid, Sharah Yasharahla, and Chris Hasten for providing stimulating discussions on this work through peer group discussions. Additionally, helpful communications with the thesis committee are acknowledged. This work was supported by the LLNL Research Collaborations Program for HBCU's and MI's. Dr. Kennedy Reed is acknowledged for directing and supplying this support. The author is indebted to Dr. Michael Williams for providing the opportunity to explore this area of science, also for his critical proof-reading of the manuscript as well as continuous beneficial discussions throughout this work.

TABLE OF CONTENTS

LIST OF FIGURES

LIST OF TABLES

CHAPTER 1

INTRODUCTION TO PHOTOLUMINESCENCE

Photoluminescence (PL) is the spontaneous emission of light from a material under optical excitation [1]. The PL technique is commonly used because of the simplicity of its process. When light of sufficient energy is incident on a material, photons are absorbed and electronic excitations are created. Eventually, these excitations relax and the electrons return to the ground state. If radiative relaxation occurs, the emitted light is called Photoluminescence. This light can be collected and analyzed to yield a wealth of information about the photoexcited material [1]. For instance, the PL *spectrum* provides the transition energies, which can be used to determine electronic energy levels. Also, the PL *intensity* gives a measure of the relative rates of radiative and nonradiative recombination. Furthermore, variation of the PL intensity with external parameters like temperature and applied voltage can be used to characterize the underlying electronic states and bands [2].

PL is commonly used to probe the composition and quality of samples. PL techniques offer support in the effort to design better semiconductor devices and to improve production efficiency. PL has little effect on the surface under investigation, and as measurements do not rely on electrical excitation or detection, sample preparation is minimal. Since the technique is optically based, PL is particularly attractive for

material systems having poor conductivity or undeveloped electrical contact and junction technology [1,3].

In short, the PL technique has advantages over other surface techniques in that it is simple, versatile, powerful, relatively rapid, the measurement is nondestructive, and it requires no elaborate sample preparation [3]. Figures 1 and 2 provide a pictorial representation for understanding this analytical technique. As seen in Figure 1, the instrumentation required for ordinary PL work is modest: an optical source and an optical power meter or spectrophotometer. Figure 2 provides an energy diagram of the PL process with energy increasing in the vertical.

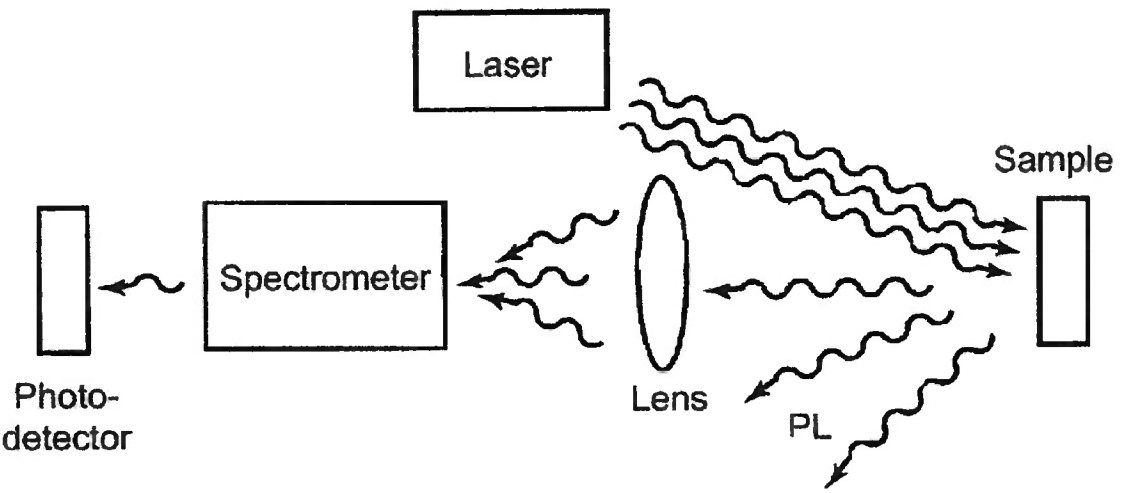

Figure 1. Pictorial representation of the PL process. Laser light is incident on the sample which then emits luminescence in the near IR wavelength. The luminescence goes through an optical setup which collects, collimates and focuses the light onto a detector. The detector then transmits the data to be outputted by a computer (not shown in diagram).

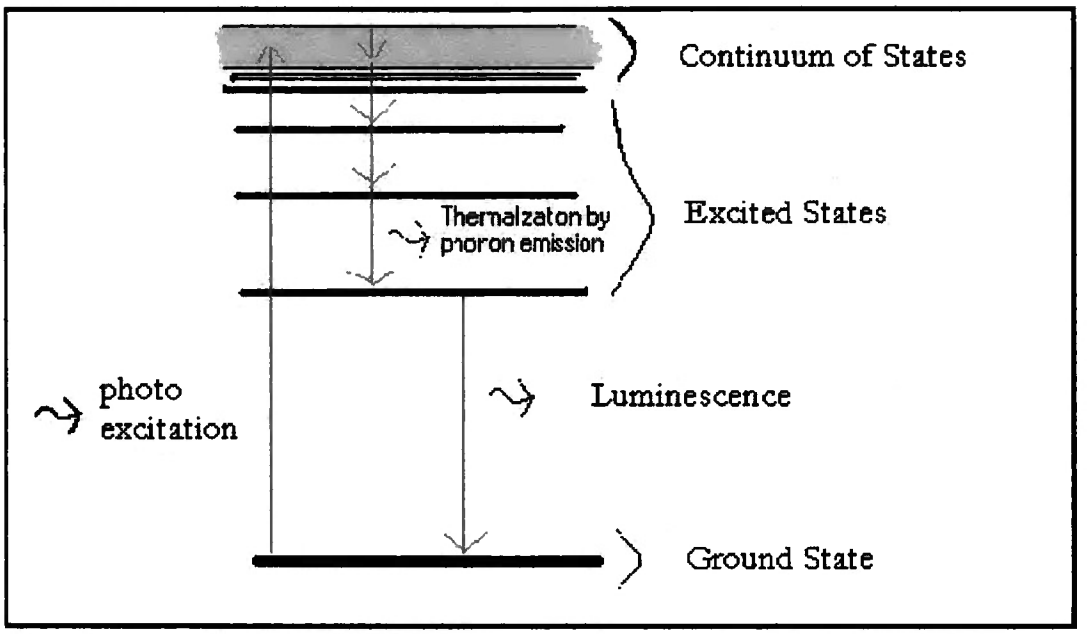

Figure 2. Simplified energy diagram of the PL process. Shows the energy levels of the system with energy increasing in the vertical

Photoluminescence characterization generates three distinct types of data. First, it generates maps of PL intensity as a function of position on a sample's surface. Secondly, it produces distributions and magnitudes of the wavelength shift of photoluminescence over the sample's surface. And finally, but most significant to this project, it can produce scans of PL intensity as a function of wavelength. These are typically used to characterize parameters such as impurity defect energy levels and bandgaps [4]. This PL system used also includes routines for such common manipulations as half-width calculations, peak labeling, background subtraction, smoothing, and derivatives.

Types of Photoluminescence

As far as surface analysis goes, there are a number of variations to this analytical technique. For instance, there is time-resolved detection. Time-resolved PL can be very

fast, which makes it useful for characterizing the most rapid processes, such as single photon counting or lifetime measurements, in a material. Another variation is energy-resolved detection. Energy-resolved photoluminescence systems can be used to determine bandgaps of solid-state materials and devices, identify defects and impurities, and analyze recombination mechanisms.

In this project, the two forms of PL studied are room temperature (RT) and low (or liquid nitrogen (LN)) temperature (LT). The difference between the two is simple – temperature. In one setup data or images of the sample are taken at room temperature; while in the other, using a cryostat, the sample temperature is reduced to that of LN where information is obtained.

Applications of Photoluminescence

In some cases, photoluminescence is used interchangeably with fluorescence and is, therefore, often associated with toys and novelties such as "glow-in-the-dark" Frisbees and yo-yo's and illuminated EXIT signs. However, in surface physics there are several potential and current uses of the PL technique – most of which have already been mentioned but will be explained further.

1. Bandgap Determination: The most common radiative transition in semiconductors is between the lowest lying states in the conduction band and the highest lying states in the valence bands. The energy difference is known as the bandgap energy. Bandgap determination is particularly useful when working with new semiconductors, and is particularly suitable for the characterization of III-V material that is to be used for optoelectronic devices such as laser diodes, light-emitting diodes, and photodiodes. Hence, PL spectroscopy provides electrical (as

opposed to mechanical) characterization and is a selective and extremely sensitive probe of discrete electronic states. Hence the most common use of PL is to help determine bandgap energies via band-to-band transmissions [1, 5].

2. Impurity and Defect Detection: In semiconductors, radiative transitions involve localized defect levels. The associated PL energy, intensity and linewidth can be used to identify specific defects and their concentration [1]. Further details of this application will be provided in chapter 4.

3. Quality of Material: Coupled with the above, localized defect levels detrimental to the surface of the material are often associated with nonradiative processes. Thus, material quality can be measured by quantifying the amount of radiative recombination [4]. A thorough analysis also helps to understand the underlying physics of the recombination mechanism.

4. Real Time Surface Modification: Because PL can be used to study virtually any surface in any environment, it can be used to monitor changes induced by surface modification. For example, unlike most surface characterization techniques, PL is generally not sensitive to the pressure in the sample chamber. Hence, it can be used to study surface properties in relatively high-pressure semiconductor growth reactors [1].

5. Unique Investigation Technique: PL is one of the only techniques available for studying fast transient behavior in materials [1]. In addition, photoluminescence excitation (PLE) is frequently used to study epilayers on opaque substrates because absorption is not feasible [1].

6. Growth Monitoring: In the effort to design better semiconductor devices and improve production efficiency at the manufacturing level, PL analysis can verify that specified growth parameters are being maintained from sample to sample and from run to run [4].

Advantages and Limitations

The advantages of PL analysis derive from the simplicity of optical measurements and the power to probe fundamental electronic properties. On the other hand, the chief drawback follows from the reliance on optical techniques: the sample under investigation must emit light. Indirect-bandgap semiconductors naturally have low PL efficiency. Nonradiative recombination tends to dominate the relaxation of excited populations in these materials. This problem can be augmented by poor surface quality, where rapid nonradiative events may occur. Nevertheless, once a PL signal is detected, it can be used to characterize both radiative and nonradiative mechanisms [1].

Another shortcoming is the difficulty in estimating the density of interface and impurity states. When these states have radiative levels, they are readily identified in the PL spectrum, and the size of the associated PL peaks provides a relative measure of their presence in the sample. However, measuring the absolute density of these states is a far more formidable task and typically requires an exhaustive analysis of the excitation intensity dependence of the PL signal [1]. A further limitation is the temperature dependence. Even though PL work can be conducted at room temperature, some information is best obtained at lower temperatures where spectral features are sharper and more intense [4].

CHAPTER 2

THE PHYSICS OF NANOSCALE STRUCTURES

In 1965 Gordon E. Moore co-founder of the Intel Corporation made a simple observation that circuit densities of semiconductors had and would continue to double on a regular basis. Although in subsequent years, the pace slowed down a bit and data density has doubled approximately every 18 months. Therefore, not only was his observation validated, but has since been defined as "Moore's Law" [6].

In accordance with Moore's Law, there is a continuing increase and rise in demands for advanced electronic and photonic devices and systems to provide networks, switching systems, and computer systems with devices and components of high speed and high capacity [7]. In recent years this demand has led to a growing interest in nanoscale technology and stems from the remarkable effects that may arise from the critical size reduction [8]. Interesting novel properties (catalytic, magnetic, ferroelectric, mechanical, optical and electronic) occur as the dimensions are reduced from a practically infinite (and periodic) solid crystal to a system composed of a relatively small number of atoms.

Nanoscience is currently one of the most dynamic and rapidly developing areas of interdisciplinary research. As nanotechnology continues to develop, multiple definitions of this emerging science have been offered. However, nanoscale surfaces can be broadly defined as substrates in which the typical features have dimensions in the

range of 1-100 nanometers. The behavior of physical systems and phenomena is therefore confined to near atomic, molecular, or macromolecular dimensions.

Properties of Nanoscale Structures

The properties of nanoscale structures – and the development of nanoscale devices based on these properties has been studied experimentally in detail by a number of groups [7 – 22]. Investigation of properties such as structural, electronic, mechanical, or optical has been a fundamental part of research in physics. For instance, details such as crystal structure, lattice constant, binding and cleavage properties, and molecular and crystal densities fall under structural properties. Thermal properties of solids can lead to calculation of specific heat or heat capacity; while optical properties of materials at the nanoscale is a key aspect to develop new devices and systems for future photonics and optical communication applications.

Semiconductor Nanostructures

Although a variety of materials can be used in the production of nanoscale devices, recently, one main focus has been on low dimensional semiconductor structures, so-called nanostructures. Of late, semiconductor heterostructures have been used extensively in many aspects of information and telecommunication technologies. The evolution and revolution of semiconductor heterostructures leading to microscale structures and nanoscale structures have started revealing many new phenomena, such as quantum interference effects, tunneling effects, and bandgap variations for applications of new and novel functions [7, 8].

Semiconductors are defined as materials whose ability to conduct electricity (dependant on the bandgap) falls between that of conductors and insulators (see Figure

3). In this study, the sample used is known as a *compound semiconductor*; which is a semiconductor formed using two or more elements. Compound semiconductors do not appear in nature; they are synthesized using primarily elements from groups II through VI of the periodic table. The compound semiconductor used for this project is gallium arsenide, GaAs, a *III-V Semiconductor,* which is synthesized using elements from column III and column V; other examples are: GaP, GaN, GaAlAs. The most common semiconductors have diamond or zincblende structures. Their basic structural properties for a unit cell can be found in Table 1, while an example of the cubic unit cell for these structures can be seen in Figure 4.

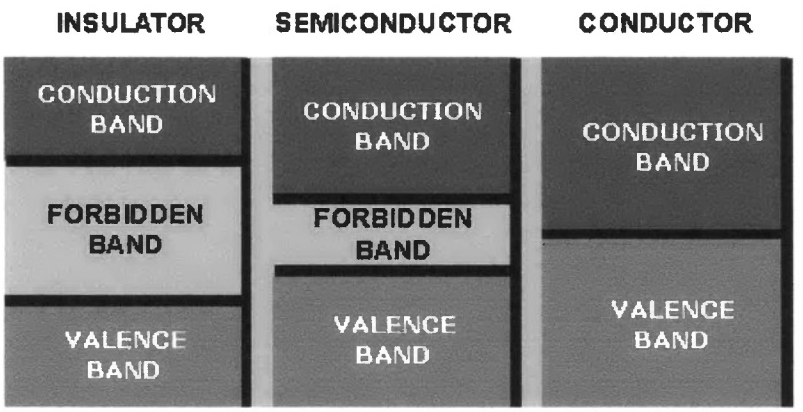

Figure 3. Bandgap difference for conductors, semiconductors, and insulators

Table 1. Structural properties of a cubic unit cell for diamond and zinceblende lattice structures

Tetrahedral coordination	Each atom has 4 nearest-neighbors (nn)
Basis set	2 atoms
Primitive lattice	Face centered cubic (fcc)
Diamond or Zincblende	2 atoms per fcc lattice point
Diamond	2 atom types are the same
Zincblende	2 atom types are different

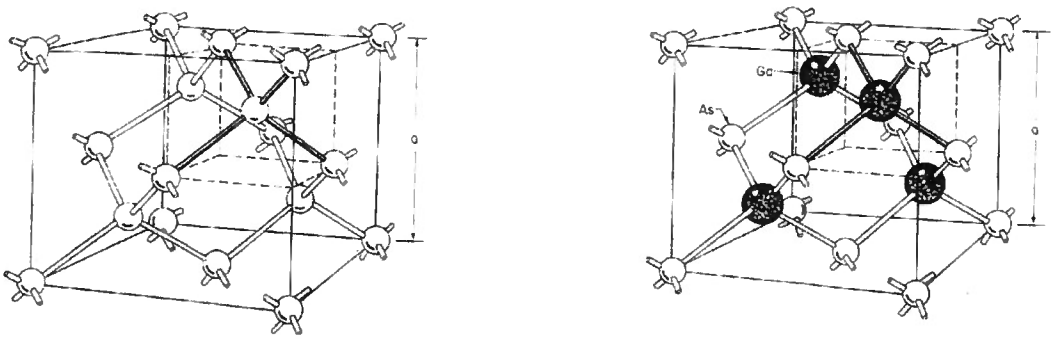

DIAMOND **ZINCBLENDE**

Figure 4. Diamond and zincblende unit cells

A degenerate semiconductor is so heavily doped that its Fermi level is closer to one of the band edges (either conduction or valance) so that the material acts essentially like a conductor rather than a semiconductor. Materials that crystallize in the diamond or the zincblende structures are representative of *degenerate* semiconductors. These materials can be further categorized as *direct* or *indirect* semiconductors. Direct semiconductors have their conduction band minimum and valence band maximum at the

same point in momentum space. In these materials momentum is conserved for electronic transitions between the bands. Indirect semiconductors have their conduction band minimum and valence band maximum at different points in momentum space. In these latter materials, a phonon must be emitted (absorbed) to conserve momentum. Two materials that have been extensively investigated and are characteristic of direct degenerate semiconductors are GaAs and InP. Two of the best-known indirect semiconductors are germanium (Ge) and silicon (Si).

Sample Material – Gallium Arsenide

Due to the extensive amount of research done on it, Gallium arsenide, (chemical formula GaAs) is our choice material. In surface physics, GaAs is an important substance since it lies midway between the purely covalent and ionic semiconductors. Gallium arsenide (GaAs) is a compound semiconductor formed from a mixture of two elements, gallium (Ga) and arsenic (As). Gallium is a byproduct of the smelting of other metals, notably aluminum and zinc, and is rarer than gold. Arsenic is not rare, but it is poisonous and is commonly used to control rodent population. GaAs was first created by Goldschmidt and reported in 1929, but the first reported electronic properties of III–V compounds as semiconductors did not appear until 1952 [9].

Since it is a direct gap, a photon is emitted when an electron changes energy levels from the conduction band to the valance band; this makes GaAs a very useful material for the manufacture of light emitting diodes (LEDs) and semiconductor lasers. Alternatively, an incident photon can excite an electron from the valence band to the conduction band, allowing GaAs to be used in photo detectors. GaAs has many useful properties that make it more beneficial to use than other semiconductors. Consequently,

for a number of years, it has been the leading semiconductor compound material used in the manufacture of field-effect transistors (FETs), integrated circuits (ICs), and LEDs found in optical communications and control systems. Furthermore, the charge carriers, which are mostly electrons, move at high speed among the atoms. This makes GaAs components useful at ultra-high radio frequencies and in fast electronic switching applications. GaAs devices generate less noise than most other types of semiconductor components and, as a result, are useful in weak-signal amplification applications like cell phones. Also, alloys made from GaAs using aluminum, phosphorus, antimony, or indium have characteristics complementary to those of gallium arsenide, allowing great flexibility [2, 9, 11].

Also, GaAs cells are relatively insensitive to heat, i.e., it is a poor thermal conductor. Cell temperatures can often be quite high, especially in concentrator applications. Arsenide is a very efficient electricity-light converter, making it a good component of solar panels. One of the greatest advantages of gallium arsenide and its alloys as photo voltaic cell materials is the wide range of design options possible [9,12]. This relatively insensitivity to heat and resistance to radiation damage makes this semiconductor very advantageous for this project – as will be seen later.

Sample Structure – Quantum Well

As stated earlier, there is an ever growing interest in low dimensional semiconductor structures in the 1–100 nm range. In the vertical dimension this feature size is characteristic for quantum well (QW) and barrier layer structures whose preparation is easily achievable by modern semiconductor epitaxy techniques [13, 14]. These semiconductor quantum heterostructures have enabled quantum well lasers,

modulators, switches, logic devices, heterostructure FETs, resonant tunneling devices, and more. Results from studies have suggested that they can be useful in bringing forth new device concepts for telecommunications and information technology [9, 13, 14]. It is this aspect that allows these structures to be taken into consideration for this project. Further lateral confinement leads to quasi-1D and 0D structures, quantum wires (QWR) and quantum dots (or boxes). In contrast to 2D structures, the preparation of 1D and 0D features, wires and dots, requires the development of novel experimental techniques since optical lithography cannot reach this level of miniaturization [14].

A QW can be defined as a physical "sandwich" structure consisting of very thin layers (e.g., 10 nm) of narrower-bandgap semiconductor, surrounded by two wider-bandgap semiconductor layers. For this case, it is a region between layers of GaAs and aluminum gallium arsenide (AlGaAs). It is designed such that electrons, holes, and excitons move essentially in two dimensions. Excitons form only when the electron and hole are coupled resulting in an appropriate Bohr radius for the particular material being considered. Figure 5 shows a schematic of the band edged of a QW. The narrower bandgap layer in the structure is a "potential well" for both electrons and holes, both of which will find lower energy in that layer, hence the term "well" in "quantum well" [9].

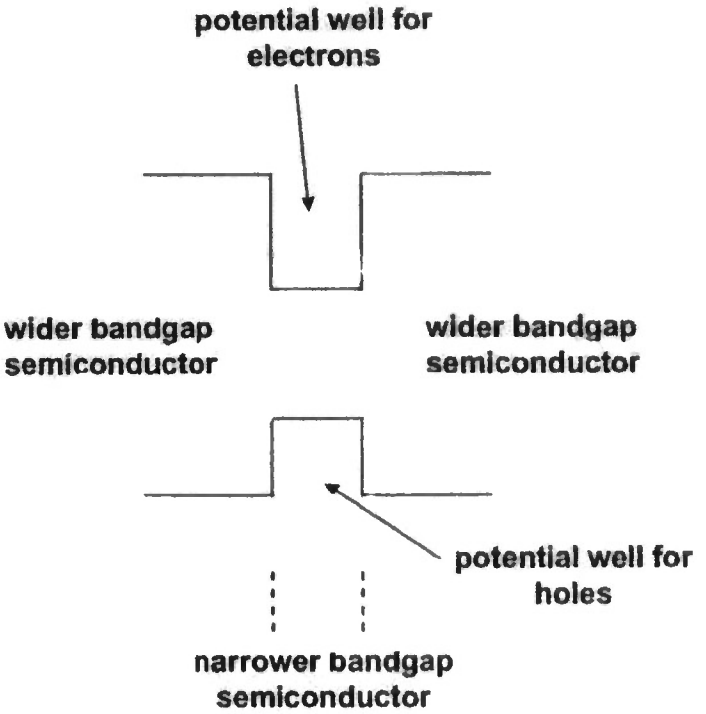

Figure 5. Description of a quantum well.

The quantum well is arguably the single most useful quantum-confined structure in optoelectronics. Aside from the uses stated earlier, quantum wells also can be used simply to adjust the effective bandgap of materials without changing the underlying material compositions, an option that is useful especially when the material growth is constrained by lattice matching requirements [9].

The three major types of QWs are finite square QWs, parabolic QWs, and triangular QWs. The QWs used in this project are unique in that from their design they are aptly named *Free Standing Quantum Wells (FSQW)*. In a FSQW, the material is patterned so as to have the quantum wells suspended horizontally between vertical support posts with air or vacuum as the barrier medium. The surface structure of a FSQW sample used in the Microelectronics lab at CAU is shown in Figures 6a – 6d.

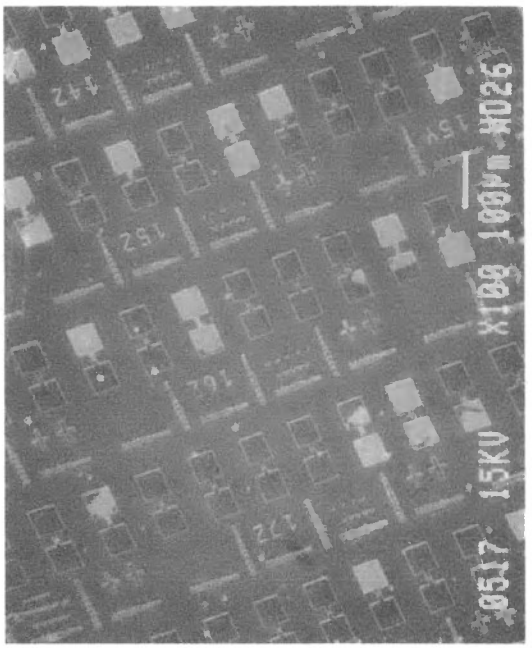

Fig. 6a

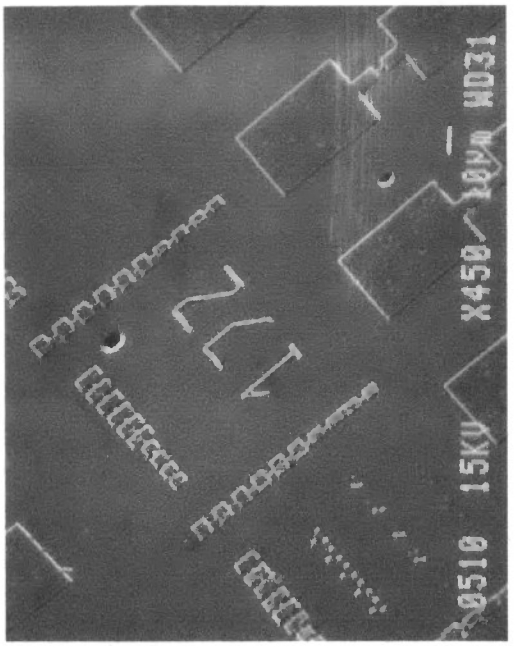

Fig 6b

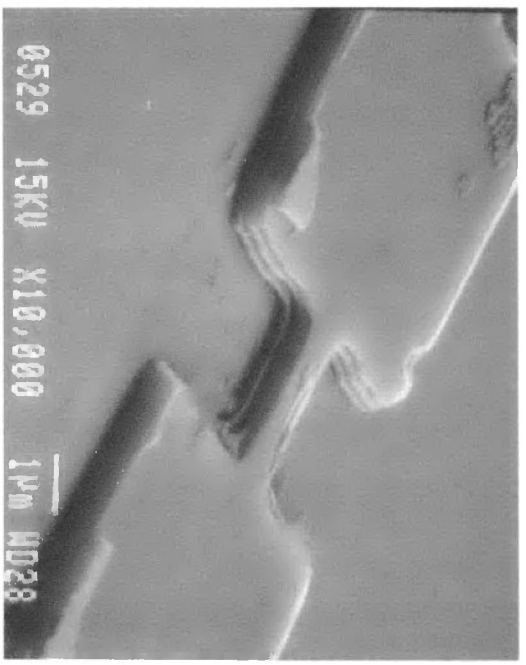

Fig. 6c

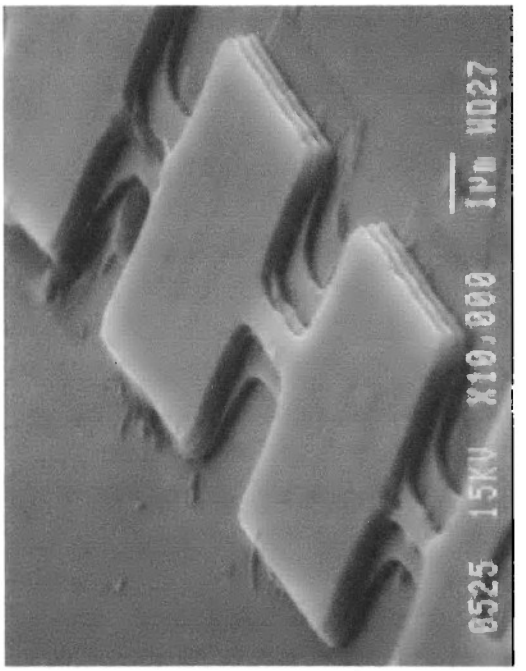

Fig. 6d

Figure 6. Examples of zoomed in areas on a sample's surface (a) 100X magnification – full area view of surface (b) section 17Z, 450X magnification – would be an ideal area for data collection (c) enlarged view of a large single well, 10,000X magnification (d) 10,000X magnification of a small chain of wells on the sample.

Sample Description

The samples used for this project were co-designed and created by Dr. Michael Williams and a team of scientists at the former AT&T Bell Laboratories. They selectively etched compositionally modulated III-V heterostuctures to produce QWs which are confined on both sides by air, vacuum or a suitable filler material [15].

The wells grown at Bell Labs are 1μm long, 0.5 – 1 μm wide and have reproducible thicknesses that range from 8-20nm with variable spacing from 100 – 200 nm between them [15]. Although Figure 6 showed the top view of a FSQW, Figure 7 presents a SEM (scanning electron microscope) micrograph of naked QWs suspended between two post structures. In this enlarged view, the three QWs shown here are 200 Å thick and are separated by 2000 Å.

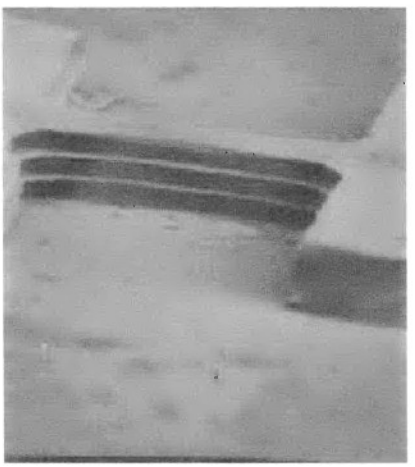

Figure 7. SEM micrograph of three naked QWs.

In summary, it can be seen that semiconductor nanostructures show many special physical properties associated with quantum confinement effects, and have many applications in the optoelectronic and microelectronic fields. Features of the PL spectrum, including line widths and splitting, provide important information on QW

interfaces. These systems are very sensitive to interface roughness because fluctuations as small as one atomic monolayer can alter the carrier confinement energy considerably. When the QW thickness varies substantially within the sampled region, a general broadening of the PL spectrum is observed. In samples with higher quality interfaces, variation in the QW thickness is limited, and recombination in different regions yields sharp, well resolved peaks in the PL [1].

CHAPTER 3

SINGLE MOLECULE SPECTROSCOPY OF NANOSCALE STRUCTURES

Defect Levels Probed With PL.

In Chapter 1, detecting impurity levels and defects is stated as one application for PL. To recap, radiative transitions in semiconductors also involve localized defect levels. The PL energy associated with these levels can be used to identify specific defects, and the intensity of the PL signal can be used to determine their concentration thereby providing information on the quality of surfaces and interfaces. The rest of the section shows how and why PL can be used to probe defect levels and the advantages of this characterization technique for this application.

Surfaces and interfaces usually contain a high concentration of impurity and defect states. Because PL often originates near the surface of a material, PL analysis is an important tool in the characterization of surfaces. Features of the emission spectrum can be used to identify surface, interface, and impurity levels and to gauge alloy disorder and interface roughness. Under pulsed excitation, the transient PL intensity yields the lifetime of nonequilibrium interface and bulk states. The utility of PL for the purpose of characterization is therefore derived from its unique sensitivity to discrete electronic states, many of which lie near surfaces and interfaces [1].

Recalling the PL process, band-to-band absorption involves elevation of an electron from the valence band to the conduction band, resulting in creation of a new pair

of charge carriers: one electron, one hole. Semiconductors are transparent to photons whose energies lie below their bandgap and are strongly absorbing for photons whose energies exceed the bandgap energy. In a direct-bandgap semiconductor, in which a non-equilibrium population of electrons and holes is excited, light will be given off through the spontaneous recombination and emission process. Carriers excited to impurity levels may also recombine to emit signature radiation [16].

Moreover, optical transitions provide direct access to the energy level structure of a system. Photons of a particular energy that are absorbed or emitted by a sample provide evidence of electronic states differing by that energy within the material. PL absorption is a good probe of the overall band structure of a system because bands have a relatively high density of states. PL emission, on the other hand, tends to favor sparse low-lying states because photoexcited carriers rapidly thermalize through bands and closely spaced states to within kT of the lowest available levels. It is this feature of PL that makes it particularly effective in the analysis of interfaces where discrete defect and impurity states abound. If the state is radiative, it will generate unique peaks in the PL spectrum. Thus, the PL measurement is a very sensitive and selective probe of such states [1].

An essential aspect of nanoscience and nanotechnology is the broad array of research activities that seek to develop new tools and techniques for the characterization and study of materials and for the fabrication and processing of nanoscale devices and systems. Chapter 2 introduced the FSQW and the fact that it is a nanoscale structure with potentially interesting properties owing to its size. It also stated how it could give insight

into the interaction of optical excitons with surface states. It is this property that invokes the topic of Single Molecule Photoluminescence (SMPL) spectroscopy.

SMPL is a subset of the field of Single Molecule Spectroscopy (SMS). SMS has grown over the past decade to the status of a powerful technique for exploring the individual nanoscale behavior of molecules in complex local environments. At present, the impact of SMS spans several fields, from physics to chemistry, to biology, and the number of applications continues to expand. SMS allows *exactly one* molecule hidden deep within a sample to be observed by using tunable optical radiation. To probe the molecule, a light beam (typically a laser) is used to pump an electronic transition of the one molecule resonant with the optical wavelength and the resulting optical absorption is detected either directly or indirectly by fluorescence excitation. Detection of the single molecule of interest must be done in the presence of billions to trillions of solvent or host molecules and in the presence of noise from the measurement itself [17].

Moerner discusses a number of advantages to this technique [17]. For instance, SMS is able to provide new information by completely removing the standard ensemble measurements that yield the average value of a parameter for a large number of (presumably identical) copies of the molecule of interest. This allows construction of a frequency histogram of the actual distribution of values (i.e., the probability distribution function) for an experimental parameter, which contains more information than the average value alone. For example, the shape of the full distribution can be examined to see if it has multiple peaks or whether it has a strongly skewed shape. Such details of the underlying distribution become crucially important when the system under study is heterogeneous [17]. Fortunately, a single molecule can be a local reporter of its

"nanoenvironment", that is, of the exact constellation of functional groups, atoms, ions, electrostatic charges, and/or other sources of local fields in its immediate vicinity. Another advantage of SMS measurements is that they remove the need for synchronization of many single molecules undergoing a time-dependent process. For example, a large ensemble of molecules undergoing intersystem crossing events must be synchronized in order to measure the lifetime [17]. A final reason for the use of single-molecule techniques is the possibility of observing new effects in unexplored regimes. For example, several single-molecule systems have unexpectedly shown some form of fluctuating, flickering, or stochastic behavior. The absorption frequency of the single molecule can change as a result of a change in its photophysical parameters or a change in local environment; this behavior has been termed "spectral diffusion" and it can produce spectral shifts or fluctuations. Such fluctuations are now becoming important diagnostics of the single-molecule regime, and they provide unprecedented insight into behavior which is generally obscured by ensemble averaging [17].

The past few decades have witnessed a dramatic increase in interest in the "nanoworld" of single atoms, ions, and molecules, for both scientific and technological reasons. There have been several successful lines of research related to SMS: (i) the spectroscopy of single electrons or ions confined in electromagnetic traps, (ii) scanning tunneling microscopy (STM) and atomic force microscopy (AFM) of atoms and molecules on surfaces, (iii) the study of ion currents in single transmembrane channels, (iv) single polymer or DNA chains with high concentrations of fluorophores, and (v) force measurements on single molecular motors using optical traps. Other examples of research exploring these fields can be found in references [18-20].

In related works, Dr. Thomas Huser and his colleagues have done a number of projects concerning SMS. In one case, single molecule confocal fluorescence microscopy was used to perform photoluminescence spectroscopy on single, isolated molecules of derivatives of the conjugated polymer poly (p-phenylenevinylene). They showed that the fluorescence from single chains of these electroluminescent polymers depends strongly on chain conformation [21]. Following up with that, photon pair-correlation spectroscopy was used to study the photoluminescence of single, isolated chains of the conjugated polymer MEH-PPV. They again demonstrated that the polymer conformation has strong influence on the quantum optical nature of the single chain photon emission [22].

The lateral dimension of the FSQWs is typically 1μm and therefore requires a high spatial resolution technique for characterization. The high spatial resolution of SMPL readily adapts itself for use in the study of the FSQW. Using this technique, this research allows for the exploration of electronic and optoelectronic properties of semiconductor materials, such as GaAs. It also allows for the introduction of an innovative cooling method – the low cost handmade cryostat seen in Chapter 5 – which provides an alternate spectroscopic method. In all, successful completion of the project could facilitate the development of quantum well devices for optoelectronic and photonic integrated circuit applications and provide quantitative descriptions of key phenomena which impact their performance. Devices based on such interactions are key components for areas like remote sensing, and telecommunications; and are also of interest for application in the detection and specification of chemical and biological agents.

Single Molecule Spectroscopy at Low Temperature

This rest of this chapter attempts to establish and justify the low temperature approach for the SMPL process. To achieve SMS at any temperature, one must (a) guarantee that only one molecule is in resonance in the volume probed by the laser and (b) provide a signal-to-noise ratio (SNR) for the single-molecule signal that is greater than unity for a reasonable averaging time [17].

Guaranteeing only one molecule in resonance is generally achieved by dilution. For example, at RT one need only work with roughly 10^{-10} mole/liter concentration in a probed volume of $10\mu m^3$. At liquid helium temperatures, the phenomenon of inhomogeneous broadening can be used to achieve dilution factors from ~ 10^4 to 10^5 simply by tuning the laser frequency to a spectral region where only one molecule is in resonance.

For absorption methods, achieving a low noise level from background effects follows from careful reduction of residual signals and operation at a power level sufficient to reduce the relative contribution from laser shot noise. For fluorescence methods, one must rigorously exclude fluorescent impurities, minimize the volume probed to avoid Raman scattering, and scrupulously reject any scattered radiation at the pumping wavelength.

The SMPL apparatus at LLNL is configured to operate at RT. A suitable modification was done to enable liquid nitrogen temperature operation. To do this, a fairly cheap hand-made cryostat was designed and constructed, such that, when tested, it took the sample down to a steady temperature of 101K. The details of this approached will be discussed in the experimental material presented in Chapter 5.

The low-temperature PL technique is of significant importance for a number of reasons. For instance, although a considerable amount of photoluminescence work has been conducted at RT, some information is best obtained at lower temperatures where spectral features are sharper and more intense; and hence, it reveals details of semiconductor properties that are unresolved at RT [4]. Also, with respect to the previous section, LT PL provides a better means to determine the quality of the material by identifying impurities and their concentrations.

In addition, it is known that at low temperatures, excitation states are the final stage in the electronic excitation relaxation energy, which is affected in a large measure by exciton interaction with defects and impurities. The characteristics of exciton luminescence (the presence of specific lines, their shape, intensity, half-width, decay time) provide a sufficiently correct idea of the dynamics of nonequilibrium carriers in GaAs crystals and, therefore, permit one to gain an understanding of the extent to which they are effected by process involving various defects in the material [23]. Literature on the subject suggests that the effect of the defects can be eliminated by reducing the sample temperature below their associated activation energies. To explain the enhanced resolution, since PL deals with electrons, we can apply the Fermi equation to it. The electrons in a semi conductor are fermions, and so they follow Fermi-Dirac statistics. The probability of a particular energy state ε being occupied is therefore

$$f_{FD}(\varepsilon) = \frac{1}{e^{(\varepsilon-\varepsilon_F)/kT}+1}$$

This distribution function takes into account that no two fermions may have the same wave function (occupy the same state). In a system consisting of N electrons at zero

temperature, all available states are occupied up to the Fermi energy level, ε_f. Furthermore, the temperature is related to the activation energy, which in turn is related to the number of accessible energy states. If the temperature is lowered, the activation energy is constant, and the number of accessible sites decreases. This in turn allows for improved signal to noise ratio in the luminescence from lower lying states of the sample surface.

CHAPTER 4

PROPERTIES OF GaAs INVESTIGATED

Band Structure of GaAs

Many of the electrical and optical properties of a pure semiconductor can be explained in terms of a band structure, which is the energy E(**k**) of an electron expressed as a function of its wave number vector **k**. Information on GaAs band structure and the energy levels associated with the band edges is summarized in Table 1. The energy band diagrams of semiconductors are rather complex. The detailed energy band diagram of GaAs is shown in Figure 8. The energy is plotted as a function of k along the main crystallographic directions in the crystal, since the band diagram depends on the direction in the crystal. The energy band diagrams contain completely-filled, completely-empty or partially filled bands. Several properties depend only on the form of the valence band maximum or minimum of the conduction band, so knowledge of these alone is of great value. The rest of this section discusses properties of the conduction and valence bands of GaAs, and some examples of basic parameters obtained.

Table 2. Basic parameters of GaAs band structures and energy levels associated with the band edges

Energy gap, $E_{G,\,opt}$ (300K) $E_{G,\,opt}$ (4K) $E_{G,\,el}$ (0K)	1.424 eV 1.517 eV 1.4 eV
Energy separation ($E_{\Gamma L}$) between Γ and L valleys	0.29 eV
Energy separation ($E_{\Gamma X}$) between Γ and X valleys	0.48 eV
Energy spin-orbital splitting	0.31 eV
Intrinsic carrier concentration	$2.1 \cdot 10^{6}$ cm^{-3}
Intrinsic resistivity	$3.3 \cdot 10^{8}$ Ω·cm
Effective conduction band density of states	$4.7 \cdot 10^{17}$ cm^{-3}
Effective valence band density of states	$9.0 \cdot 10^{-18}$ cm^{-3}

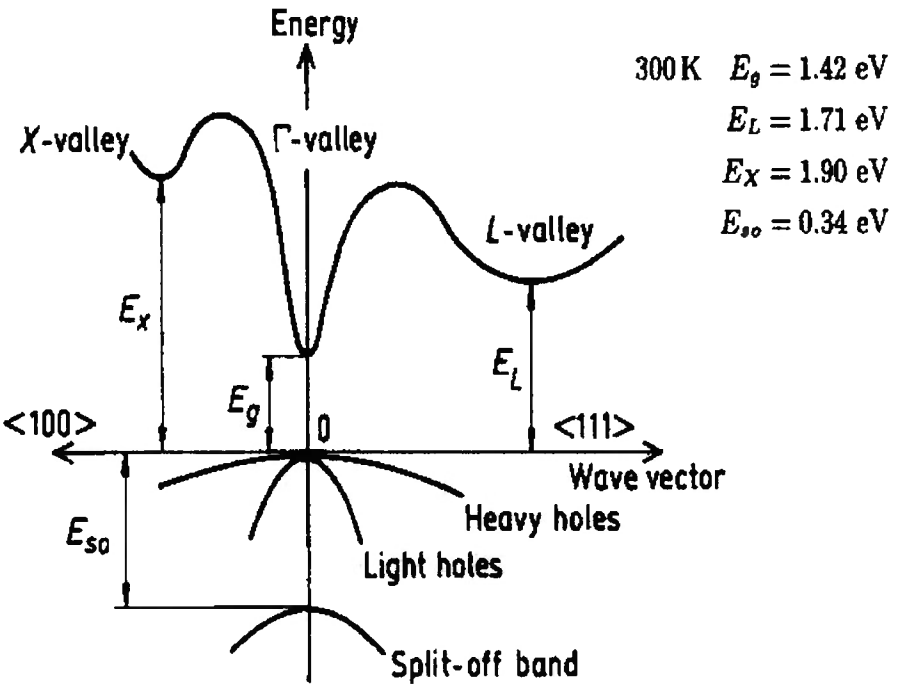

Figure 8. Band Structure and carrier concentration of GaAs at 300K

The valence band of GaAs is degenerate at the center of the zone. There is a heavy-hole band and a light-hole band, and also a third band split off by spin-orbit interaction. Although GaAs is a direct semiconductor, because of the lack of inversion symmetry in the GaAs crystal, the degeneracy of the heavy-hole bands will be split and their maxima will not lie exactly at the zone center, but a small distance away [24]. In GaAs more than one subband of the conduction band plays a role. Experimental evidence indicates that, along with a minimum found at the zone center, there are minima lying in the [111] and [100] directions in *k*-space, with an energy somewhat above that of the minimum at $\mathbf{k} = 0$ [24, 25]. Their average values can be found in Table 1.

The first basic parameter to be examined is the forbidden gap E_G, (see Figure 3). Table 2 contains 3 kinds of values. Two of these are obtained from optical measurements and the other from electrical measurements. The values depend on linear extrapolation from high temperatures to 0K. In GaAs, the transitions for which E_G is the threshold energy are direct transitions from the valence band into the lowest (000)-minimum of the conduction band [25].

Absorption peaks obtained from structures occurring in the infrared spectrum of p-type material, and attributed to transitions between the three valence bands have been observed [24]. The photon energies at which the bands occur are independent of the acceptor impurity and of the density of holes, nor do n-type samples show this structure. A peak at 0.42eV is attributed to transitions between the spin-orbit split-off band and the heavy-hole band. A peak at 0.31 (seen in Figure 8a) is attributed to transitions between the split-off band and the light-hole band, and the absorptions beginning at about 0.25 eV to transitions between the light- and heavy-hole bands [24].

Before the density of carriers in a semiconductor can be calculated, the number of available states at each energy level must be found. The number of electrons at each energy level is then obtained by multiplying the number of states with the probability that a state is occupied by an electron. Since the number of energy levels is very large and dependent on the size of the semiconductor, the number of states per unit energy and per unit volume can be calculated first. The density of states in a semiconductor then equals the density per unit volume and energy of the number of solutions to Schrödinger's equation. However, a few assumptions must be made. Assume the semiconductor can be modeled as an infinite quantum well in which electrons with effective mass are free to move, the energy in the well is set to zero. The semiconductor can assume any shape. This assumption does not affect the result since the density of states per unit volume should not depend on the actual size or shape of the semiconductor. A more in-depth discussion can be found in [24]. Experimental values of the conduction band density of states have ranged between 5×10^{16} electrons cm^{-3} to 7×10^{17} electrons cm^{-3}. The effective value is found in Table 2. The effective value for the valence band is also provided.

Crystal Defects

Three questions will be tackled in this section, namely: *What are the main types of defects? How do defects come about?* and *What effect do defects have on the sample?*

It is useful to think about solids in terms of a regular repeating pattern of planes of particles. Yet, solids are seldom perfectly ordered and no semiconductor crystalline material is perfect. In spite of the efforts to control crystal growth, GaAs crystals contain a number of crystal defects, dislocations, and impurities. These defects can have either

desirable or undesirable effects on the electronic properties of GaAs [9]. For instance, carbon and oxygen are the main impurities that exist in GaAs, which contribute to low bulk resistivity if they are not counteracted. The nature of these defects and the observed effects are determined by the method of their incorporation into the material and the general growth conditions [9]. In general, the main types of defects are point defects and dislocations.

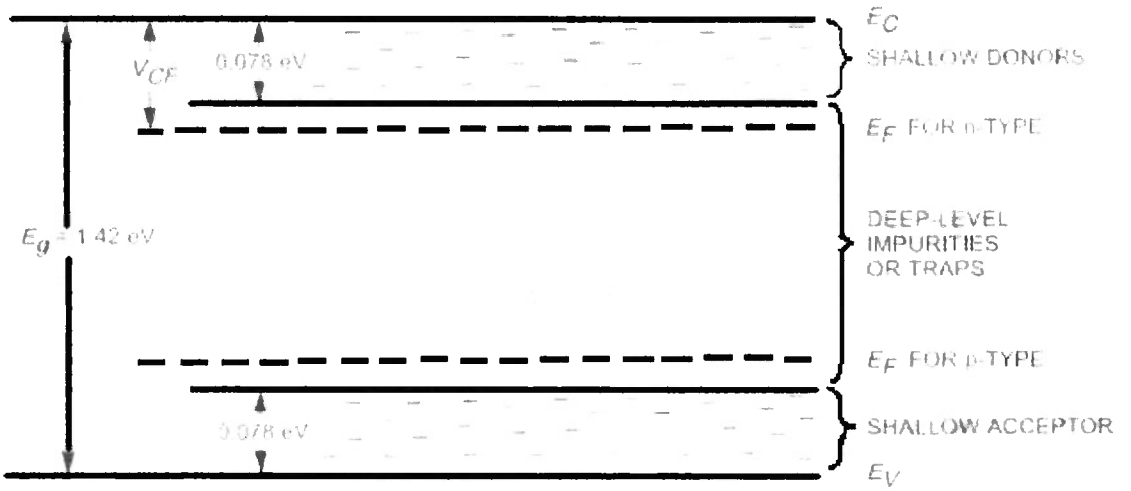

Figure 9. Energy band diagram of GaAs with the addition of impurities (shows VB max and CB min)

Localized defects of atomic dimensions, called **point defects**, can occur in an otherwise perfect crystal lattice. There are four basic mechanisms for introducing a point defect into the structure of a solid and can be seen in Figure 10. They include vacancies, interstitials, misplaced atoms, and intentionally or inadvertently introduced impurities.

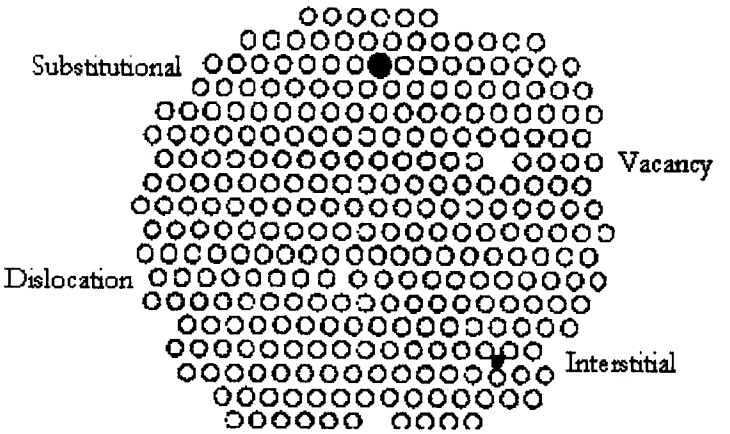

Figure 10. Four basic mechanisms for introducing defects into the structure of a solid

Point defects distort the lattice and provide a way for atoms to move about the solid; for instance, atoms can move from a lattice site into a vacancy, creating a new vacancy, as shown in Figure 11. Distortions of the crystal lattice often occur when impurities are added to a solid. As a result, point defects often determine the properties of a material for instance the effect these defects have on the electronic properties of the material and the strong relationship between diffusion and the number and type of defects in the crystalline material. They can therefore change the ease with which a material conducts electricity, its malleability, or its ductility [24].

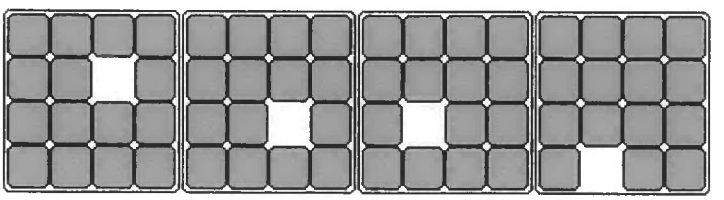

Figure 11. Example of formation of a vacancy in a solid

Point defects can further be divided into two main categories: Intrinsic and Extrinsic Point defects. Vacancies and interstitial defects are intrinsic point defects. An interstitial defect is when a particle forces its way into a hole and gets trapped between lattice sites. Extrinsic point defects are foreign atoms in the crystal. Chemical point defects can be introduced to the crystalline material either deliberately or inadvertently as contamination during processing. When they arise accidentally they are called impurities; however, when they are added deliberately they are called dopants. These dopants add extra electrons or holes. A semiconductor with extra electrons is called an n-type semiconductor, while a semiconductor with extra holes is called a p-type semiconductor.

A *dislocation* is an immobile one-dimensional array of point defects in an otherwise perfect crystal. They are basically extended defects where a long line or plane of atoms is out of position relative to their neighbors. Dislocations are caused by holes that are not large enough to be vacancies, and occur when the crystal is subjected to stresses in excess of the elastic limit of the material which initiates a crack at the surface. Though dislocation cracks are not necessarily straight, they tend to lie in the cleavage planes (110). A strong local impact can produce a sheet of dislocations up to several millimeters in length. If the stress is not uniform, the material on the two sides of the crack will be deformed by different amounts. If the impact lasts such a short time that the atmosphere does not penetrate into the crack, the two sides will come together again and the crack will heal. However, now the atoms on the two surfaces will not be correctly aligned and the mismatch will rearrange itself into dislocation lines [24]. The main types are edge dislocations, screw dislocations, and stacking faults. Edge dislocations look as

if an extra plane of atoms has been inserted into the crystal, but only inserted part way as seen in Figure 12. In Figure 12a the dislocation looks rather extreme, but from Figures 12b and 12c it is seen that they are fairly subtle. Yet they are, indeed, very common defects. Screw dislocations are more difficult to visualize. Figure 12d shows how a screw dislocation is produced when one side of a crystal is displaced relative to the other side. For either edge or screw dislocations a distortion is produced around the dislocation with a corresponding stress produced within the material.

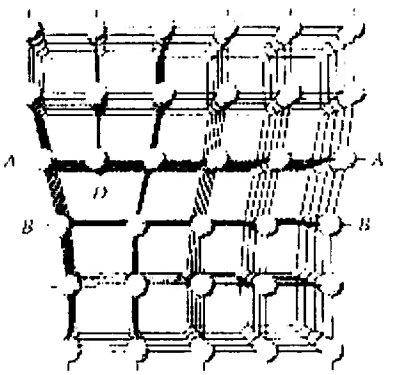

12 (a)

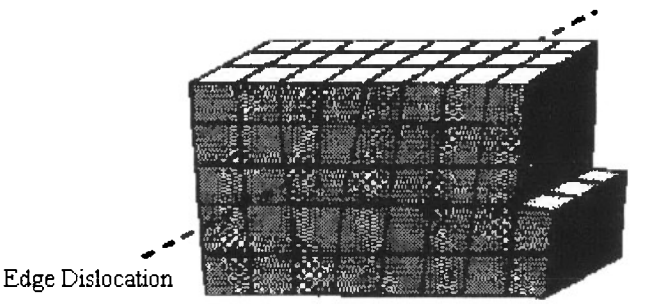

12 (b)

12 (c)

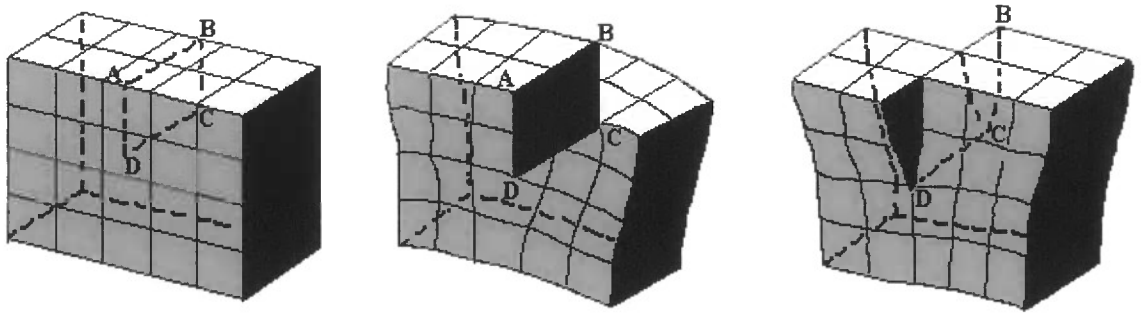

12 (d)

Figure 12. Dislocation formation in a solid (a), (b), (c) edge dislocations. (a) and (b) look as if an extra plane of atoms has been inserted into the crystal, but only part way; (c) the dislocation is hardly noticeable; (d) shows how a screw dislocation is produced when one side of a crystal is displaced relative to the other side.

Dislocations generally are introduced as a result of a temperature gradient present during crystal growth. They interact with chemical and other point defects. This interaction exists between the localized impurity atoms and the strain field in the vicinity of the dislocations. The presence of a dislocation is usually associated with an enhanced rate of impurity diffusion leading to the formation of diffusion pipes. This effect translates to the introduction of trapping states in the band gap, altering the etching properties of the wafer, and, most importantly, altering the electrical properties of the devices. Studies have shown detrimental effects of dislocations and dislocation densities on the source drain current and threshold voltage of field-effect transistors FETs, carrier concentration, and sheet resistance [26].

Effect of Impurities and Other Defects on GaAs

Many intrinsic defects are observed in GaAs. The concentration and effect of these defects are determined by the manner in which the material is grown. Intrinsic

defects in GaAs include both arsenic and gallium vacancies, where their concentration is determined by the overpressure of arsenic during processing. The effect of these vacancy defects has been observed to be neutral, deep donor-like, and deep acceptor-like. For instance, EL2, an important defect in GaAs, is present in material grown from an arsenic-rich melt. This defect is donor-like in character and is located at the middle of the energy gap. It is thermally very stable and can withstand processing temperatures up to 373K, and acts as an electron trap. The importance of this defect lies in its ability to convert p-type GaAs to semi-insulating material, and its thermal stability [9, 26].

Both impurity types, deep and shallow, are present in GaAs in the form of complexes with gallium or arsenic. Silicon and carbon are used extensively to provide p-type GaAs. Chromium (Cr) behaves as an acceptor, with an impurity level close to the center of the energy bandgap. This property makes it very useful for counter-doping n-type GaAs to make it semi-insulating. Other elements such as copper, oxygen, selenium, and tin are also used in GaAs processing to provide the desired n- or p-like behavior [9, 26]. The change in the energy band gap due to high doping levels can be seen in Figure 13. As the concentration level rises the band gap increases causing GaAs take on more properties of an insulator.

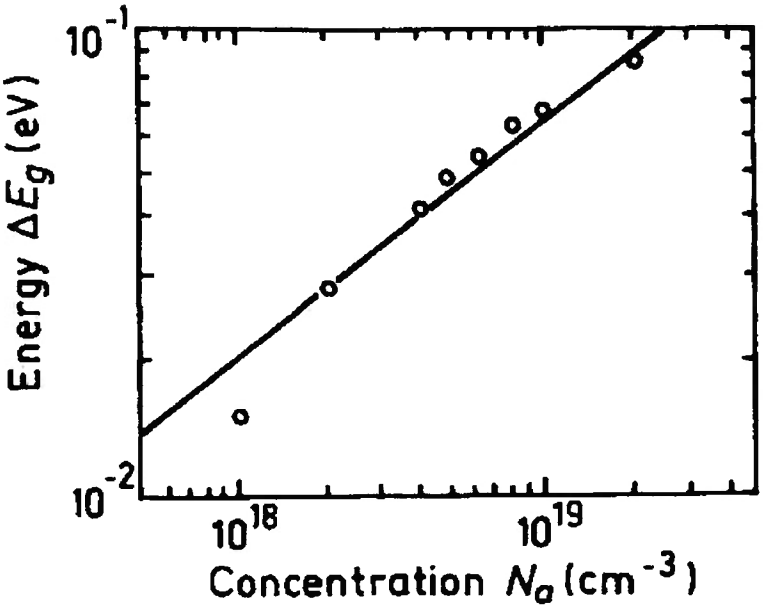

Figure 13. Graph showing effect of impurities on the energy gap of a semiconductor. The gap narrows at high doping levels.

The electrical properties of the specimen, especially when measured at low temperatures, can be greatly affected by the presence of dislocation cracks. The wall of dislocation line behaves like a sheet of material running through the semiconductors, the sheet having properties different from those of the bulk crystal. Therefore, when preparing specimens it is necessary to take precaution to avoid introducing these defects. Dislocation cracks may be produced by cutting, grinding, or even picking up with tweezers. Shaping specimens with a fine jet of abrasive powder is a technique that is found to be less likely to introduce these cracks, and the use of tweezers should be avoided [24].

Temperature Dependence of the Energy Bandgap

The energy bandgap of semiconductors tends to decrease as the temperature is increased, and vice versa. Therefore at lower temperatures a wider gap is achieved and more states are accessible to be probed. This in turn, creates more peaks in the spectrum. This behavior can be better understood if one considers that the interatomic spacing increases when the amplitude of the atomic vibrations increases due to the increased thermal energy. This effect is quantified by the linear expansion coefficient of a material. An increased interatomic spacing decreases the average potential seen by the electrons in the material, which in turn reduces the size of the energy bandgap. A direct modulation of the interatomic distance - such as by applying compressive (tensile) stress - also causes an increase (decrease) of the bandgap.

The temperature dependence of the energy bandgap, E_g, has been experimentally determined yielding the following expression for E_g as a function of the temperature, T:

$$E_g(T) = E_g(0) - \frac{\alpha T^2}{T + \beta} \qquad (1)$$

where Eg(0), α and β are the fitting parameters [27]. These fitting parameters are listed for germanium, silicon and gallium arsenide in Table 3. A plot of the resulting bandgap versus temperature is shown for germanium, silicon and gallium arsenide in Figure 14.

Table 3. Parameters used to satisfy equation 1

	Germanium	Silicon	GaAs
$E_g(0)$ (eV)	0.7437	1.166	1.519
α (meV/K)	0.477	0.473	0.541
β (K)	235	636	204

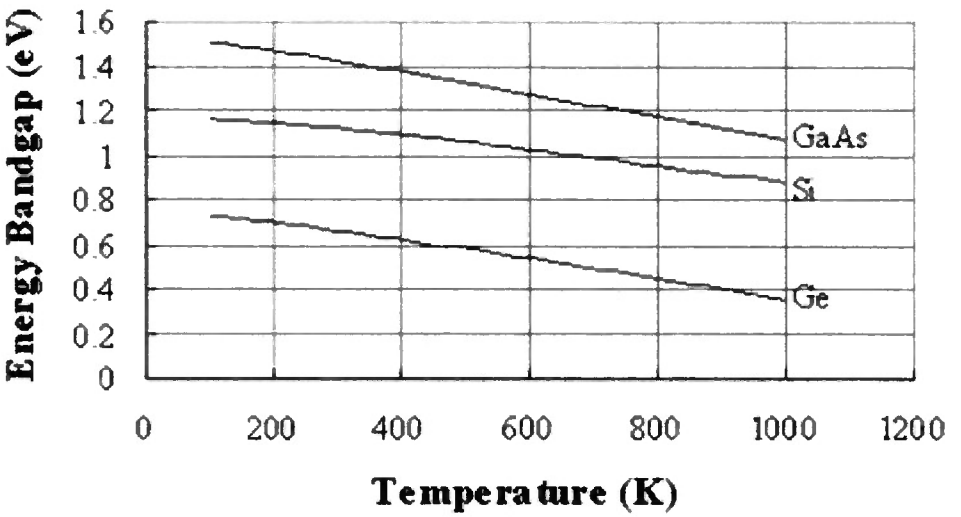

Figure 14. Graph showing effect of temperature on the energy band gap of common semiconductors: GaAs, Ge, Si (plot of Energy bandgap vs. temperature)

CHAPTER 5

EXPERIMENTAL DESIGN AND IMPLEMENTATION

This project is being done in collaboration with the Dr. Thomas Huser at Lawrence Livermore National Laboratory. His team developed a sensitive methodology of detecting light from single molecules. This SMPL process introduced in Chapter 3 offers a spatial resolution to analyze the area of interest that was not available before. In addition, there is the added advantage of having the capability of studying adsorbate interactions. This latter aspect has important ramifications for sensor technology.

Objectives

Experimentally, this project aims to develop the infrastructure to study the interaction kinetics of the quantum confined exciton states in the freestanding GaAs QW structures by LT PL using SMPL.

The basic tasks of this project are to procure samples containing GaAs free standing QWs, identify suitable regions for PL analysis at Lawrence Livermore, and analyze the structures at RT and LT. With respect to the setup, since the SMPL apparatus at LLNL is currently configured to operate at RT, the main goal is to construct a LT PL system at Clark Atlanta based on personal experience obtained at LLNL. As a result, a suitable modification that should enable LN temperature operation (77K) would be developed. In particular, one goal with this LT setup is to obtain lifetime data on the sample; which cannot be done at RT.

Preliminary Results

State-of-the-art facilities exist within LLNL to conduct a broad based investigation of QW materials. On site at LLNL a variety of optical probes, such as Raman spectroscopy, PL and Time-resolved optical spectroscopy, can be performed. Previously, PL measurements were performed on the GaAs structures at both LLNL and AT&T Bell Labs. At LLNL room temperature PL was done on the sample. At AT&T Bell Labs, spectroscopy of the freestanding GaAs (100) QWs was done with near-field optical microscopy and RT cathodoluminescence. In both these previous studies, the results were inconclusive. PL analysis showed no difference between the QW and its supporting posts. This suggests either excess recombination due to surface states in the QW region or insufficient absorption length for PL. The issue of excess recombination due to surface states in the QW region is easily resolved by LT spectroscopic measurements and time resolved optical techniques. The special requirement here is for a system with a lateral resolution of 1μm or better.

Experimental Review

As stated in Chapter 1, the fundamental process of taking PL data is the same for all temperature measurements. To recap, a laser light will strike a sample; for LT, the sample is generally mounted in some form of cryostat, which, commercially, allows the sample temperature to be varied anywhere between 4.2K and 800K. The sample absorbs the energy and excites electrons then undergoes "photo excitation". The process continues until emission or luminescence is obtained. The emitted light is then collected and focused onto the slit of a monochromator. In the monochromator the light is dispersed and the monochromatic light is then detected by a light sensitive detector. The

following section details the parameters that affect the PL signal thereby providing an explanation to the choice of experimental equipment.

Parameters Affecting the Photoluminescence Signal

The choice of excitation should be carefully considered in any PL measurement. The excitation energy and intensity will have profound effects on the PL signal. The excitation energy selects the initial photoexcited state and because the absorption of most materials depends on energy, the penetration depth of the incident light will depend on the excitation wavelength. The PL signal often depends on the density of photoexcited electrons, and the intensity of the incident beam can be adjusted to control this parameter. Although the excitation conditions must be considered carefully, the strength of the PL technique relies heavily on the flexibility that these adjustable parameters provide. This allows different excitation energies to probe different regions of the sample [1].

Since lasers are monochromatic, intense, and readily focused, they are the instruments of choice for photoluminescence excitation. For many PL applications, the excitation energy is not critical. Therefore, a relatively inexpensive HeNe or diode laser will often satisfy the basic requirement that the light exceeds the bandgap energy of the material [1]. Usually for PL, the energy of the laser comes from short-wavelength light, typically ultraviolet, i.e., argon laser, YAG lasers. At LLNL a 632nm (HeNe) laser and a 514.5nm (green) laser were the optical sources. However, at CAU, a 532 nm diode pumped solid state laser was used to excite carriers within the semiconductor sample. It is compact in size, has low power consumption, and a long operating life. The laser uses an 808nm IR diode laser to pump an Nd:YVO4 crystal. The Nd:YVO4 crystal generates a 1064nm output, which is then frequency doubled using a KTP crystal. The exit beam is

532nm (green). It has a TEM_{00} beam and linear polarization. Output power is rated as the *minimum* average output power and is suitable for many research applications. In more demanding experiments, the laser is chosen carefully to probe a particular depth or to excite a particular species in the sample.

In contrast to the excitation energy, which may or may not be important, the excitation intensity will influence the result of any PL experiment. The excitation intensity controls a critical property of the PL experiment: the density of photoexcited electrons and holes, which governs the behavior of these carriers. Each electron–hole recombination mechanism has a distinct functional dependence on carrier density. For example, the number of interface and impurity states is finite, and recombination at these sites will saturate at high excitation. In addition, the photoexcited carriers themselves can alter the distribution of interface states. Furthermore, the presence of surface adsorbates alters the intensity of the PL signal. Thus, the excitation intensity must be calibrated accurately and controlled precisely [1]. Because of the spectral region it covers (300-1700nm), the Si/InGaAs photodiode chosen for this setup can be used to detect the presence or absence of minute light intensities and can be calibrated to measure the intensity of light extremely accurately.

Chapter 3 details how PL depends quite strongly on temperature. A convenient way to cool many kinds of apparatus is to submerge them in liquid helium or liquid nitrogen. Nitrogen gas, when cooled, condenses at 77.36 K and freezes at 63.17 K. Liquid nitrogen is used in many cryogenic cooling systems and was chosen to be used at both CAU and LLNL. Liquid helium, because of its low boiling point, 4.2 K, is used in

many cryogenic systems when temperatures below the boiling point of nitrogen are needed. Liquid He temperatures are required for the highest spectral resolution.

Lastly, a factor that calls for much consideration is the required optics for a PL arrangement. At CAU, there were a number of important elements contributing to the chosen apparatus. The first was the required resolution. As the wells are 1μm in length and 0.5 - 1μm in width, a maximum laser spot size of 1 μm^2 is desirable to focus on the sample. The next aspect was imaging the wells on the monochrome TV screen. It was necessary that the microscope objective used to view the sample provided an image of the wells that was clearly distinguishable from the other wells nearby; while also providing the necessary working distance needed to incorporate all surrounding equipment. Another aim was to image the maximum size of the wells without distorting the images, so a careful choice of microscope objective is essential. The final significant factor taken into consideration was the noise reduction. For this a chopper was included in the design for phase-lock signal detection

Low Temperature Photoluminescence Setup – LLNL

The setup is similar to one used by Huser et al. [22]. On the excitation side of the setup, the 632 nm HeNe or 514.5 nm line of a water-cooled argon-ion laser serves as light source. The laser light is coupled into a single-mode optical fiber and guided to an optical table mounted above an upright optical microscope. After passing a narrow bandpass filter that rejects any Raman scattering or fluorescence from the fiber, the circularly polarized beam is directed toward a pellicle beamsplitter that reflects 10% of the beam to the microscope tube. The transmitted 90% are being dumped at a beam stop. The use of the broadband reflecting beamsplitter allows rapid switching of the excitation light source

without the need to change a dichroic mirror – at the expense of losing most of the excitation power [22]. The excitation beam is finally focused to a diffraction-limited spot by an objective lens with high numerical aperture.

On the detection side, the locally excited fluorescence is collected by the same microscope objective. The collimated beam passes the pellicle beamsplitter and is then separated in two parts by a 50/50 broadband beamsplitter cube. One arm passes a holographic notch filter and is then focused through the entrance slit of an imaging monochromator that disperses the light onto a liquid nitrogen cooled back-thinned charge coupled device camera. The other arm passes a longpass optical filter mounted in a remote controlled filter wheel. An antireflection-coated lens focuses the fluorescence onto a photon-counting avalanche photodiode (APD), whose active area with a diameter of 170 μm serves as a confocal aperture. For imaging and positioning purposes, the sample is held on a three-axis scan stage with 100μm lateral scan range and closed-loop feedback. This stage makes it possible to obtain photoluminescence images of samples by scanning them through the focus of the excitation beam. Once an image at low power has been acquired, individual spots can be addressed by the scan stage for local spectroscopy. Scan motion and data acquisition are provided by a scanning probe microscope controller equipped with a dual-channel pulse counting board.

Components Necessary to Complete Setup

An initial attempt at LLNL to lower the sample temperature to that of liquid nitrogen (77 K) was made using the following commonly available components:

- Styrofoam cup
- Clamp to hold Styrofoam cup

- SEM stub to mount the sample – this was glued to the base of the Styrofoam cup
- Liquid Nitrogen

Figure 15 shows an example of this original design for the low temperature set up. The cup was then clamped above the inverted optical microscope mentioned above. Unfortunately, the approach was unsuccessful. Two main problems were encountered. First, it was impossible to lower the sample temperature past 243K; and secondly, the vibrations produced by the boiling nitrogen made imaging the FSQW impossible. Several alternate, low cost, low temperature techniques were discussed and investigated as possible solutions to these problems. Others who have performed PL experiments and have had successful results have used commercial cryostat to vary their temperature. A commercially available optical cryostat would be ideal but none were available for loan and the cost of this item far exceeded the allotted budget.

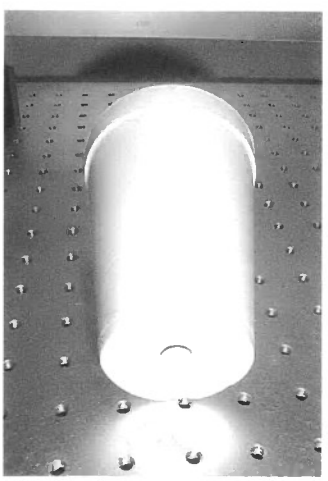

Figure 15. Original cryostat design. Styrofoam cup with an SEM stub inserted in the base.

Figures 16 – 20, present the schematics for the low-cost, low-temperature cryostats for PL measurements designed in CAU's Microelectronics lab. Figure 16 is one of the revised designs that led to the final design. This design incorporated all the necessary structures needed for the successful reduction of temperature. There is a heavier Styrofoam dewar to hold the cryogenic coolant, and a long, relatively heavy copper feed-through that allows for thermal conduction to the sample, which theoretically should help reduce the vibrations. But more importantly is the vacuum chamber which housed the sample. This, along with the pump to suck out the air, was designed to prevent the condensation formed in the previous setup from developing again on the sample surface. This condensation would most likely destroy the sample. A glass window to image our sample was also incorporated in the design. The only problem with this design was that there was a weight limitation that one element, the flange, exceeded.

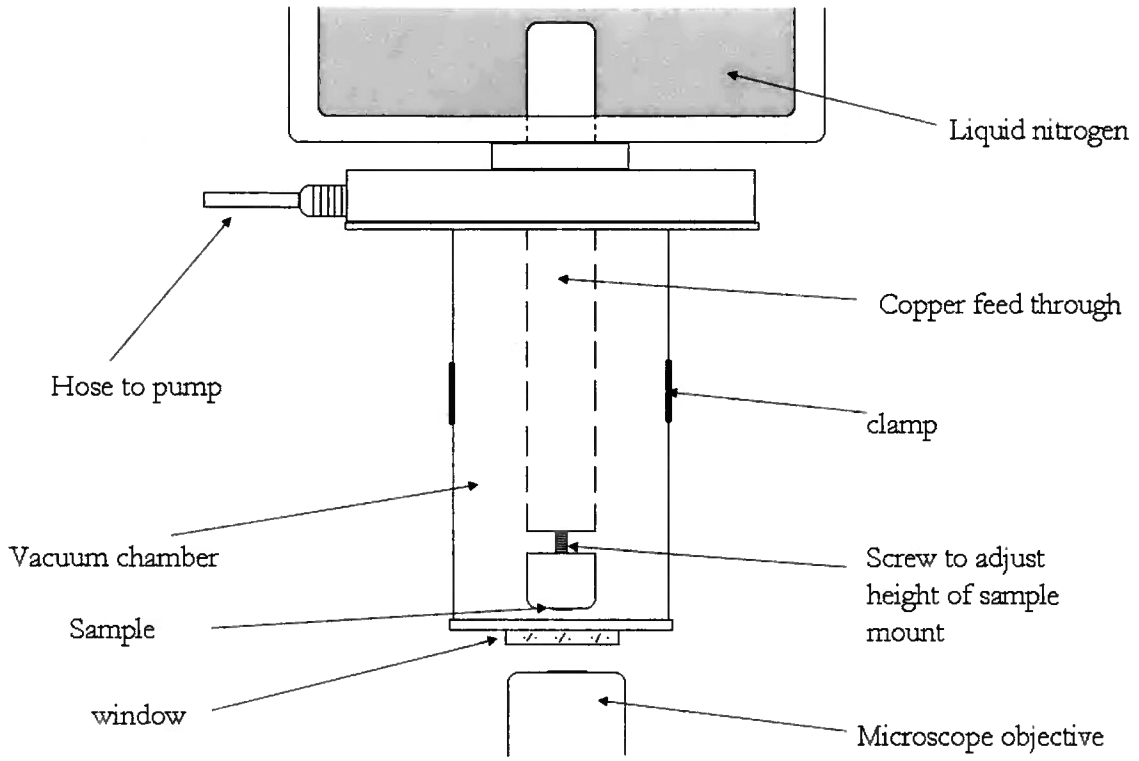

Figure 16. A revised design before obtaining final design. The major consideration here was that this design did not meet the weight limitations.

In the final revision, instead of the significantly heavy flange, an aluminum tube (see Figure 17) was found to replace it. This substantially reduced the weight of the cryostat. There was a need to pump out the system to create the vacuum. The advantage the flange had over the Al tube was the holes where a pump could easily be attached. However, this was solved by drilling a hole on the side of the tube (also Figure 17).

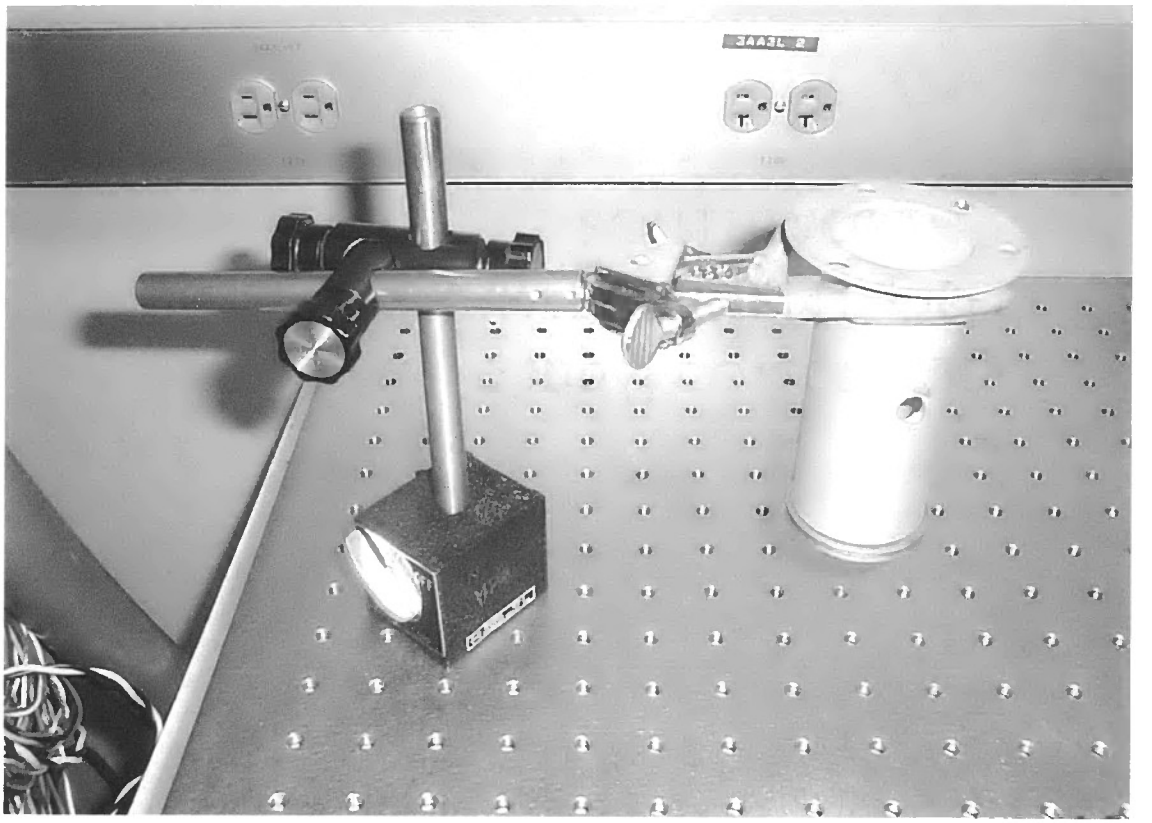

Figure 17. Aluminum vacuum tube for new setup. The hole in the side is for the Swagelok fitting that attaches to the hose and the thermocouple. Allowed us to meet our weight restrictions.

A T-shaped Swagelok fitting, from which on one side a hose could be connected, and on the other, a thermocouple could be inserted, would then be screwed into the hole. The thermocouple allowed the sample temperature to be checked. Figure 18 shows the viewport for the cryostat. A hole was drilled on a copper gasket and a glass plate glued to the surface. A copper O-ring was then attached to the top to prevent scratches or other damage to the plate if it should be place face-down on a surface.

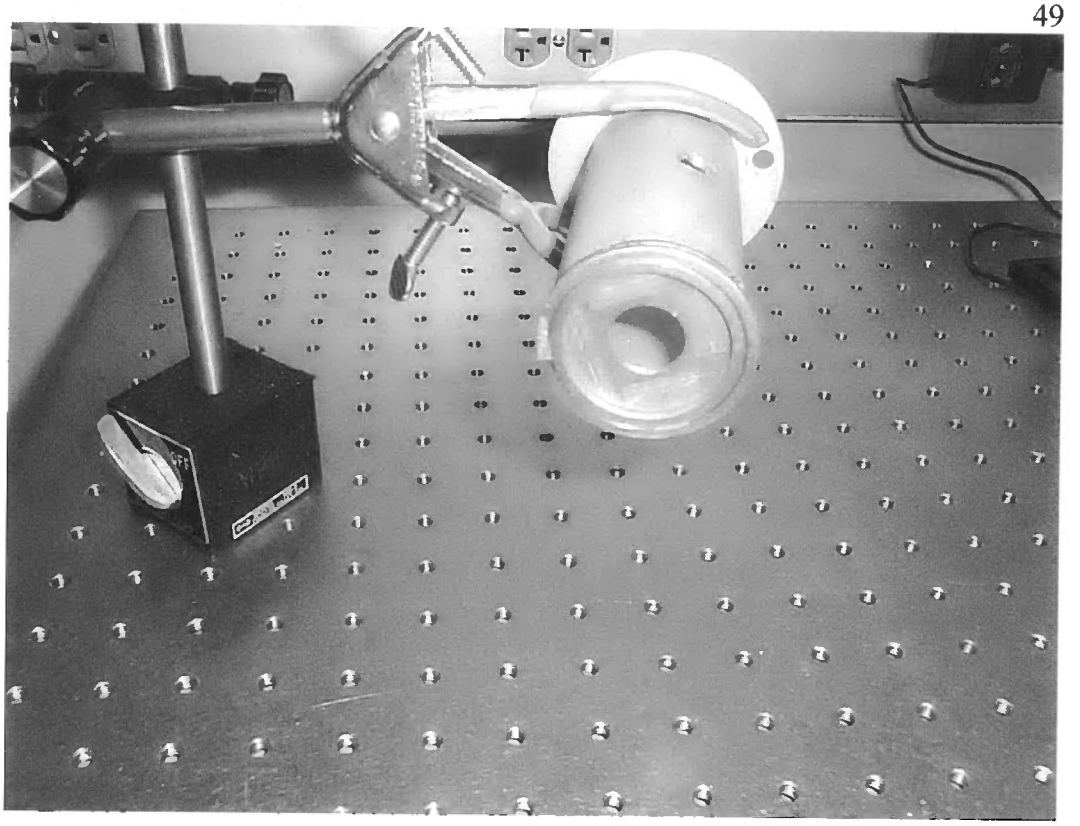

Figure 18. Window (view port) for the sample to be imaged by the microscope

Figure 19 shows the completed setup once everything has been attached. It also shows an initial test where the sample was able to be reduced to ~101K. Next, Figure 20 shows the inner workings of this completed and final design. It has the same basic structure as the original revised design. The only significant difference between the final design and the original ideas is the copper O-ring at the base of the Styrofoam dewar and the vacuum O-ring on the surface of the Al tube. These two elements were included to create a tight seal between the Styrofoam dewar and the vacuum chamber. This would allow for a quick changing of the sample, should the need arise, and also allow for an easy dismantling of the setup if corrections were needed during data collection.

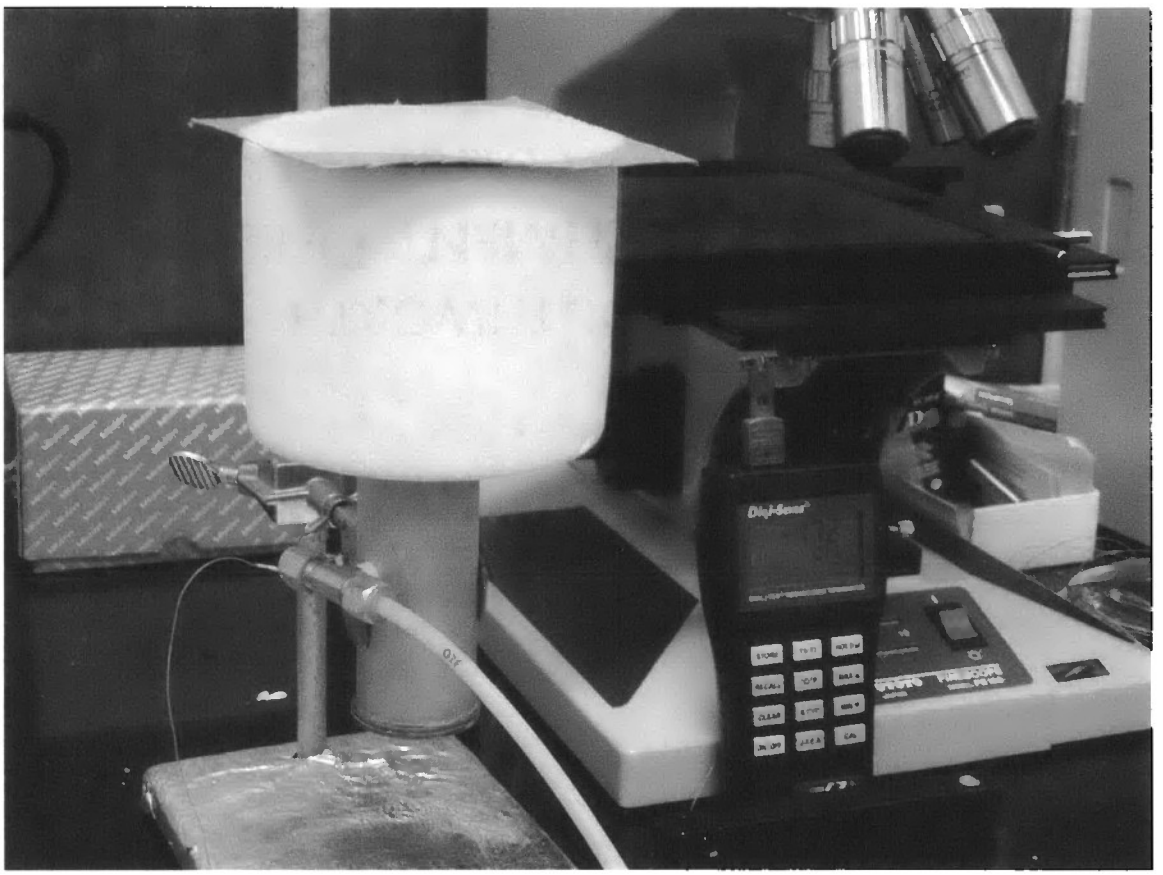

Figure 19. Completed design of the cryostat. The Styrofoam dewar sits on top of the vacuum tube. [The whole setup is then held over the microscope objective seen in Figure 21]. The thermocouple meter reads -172°C.

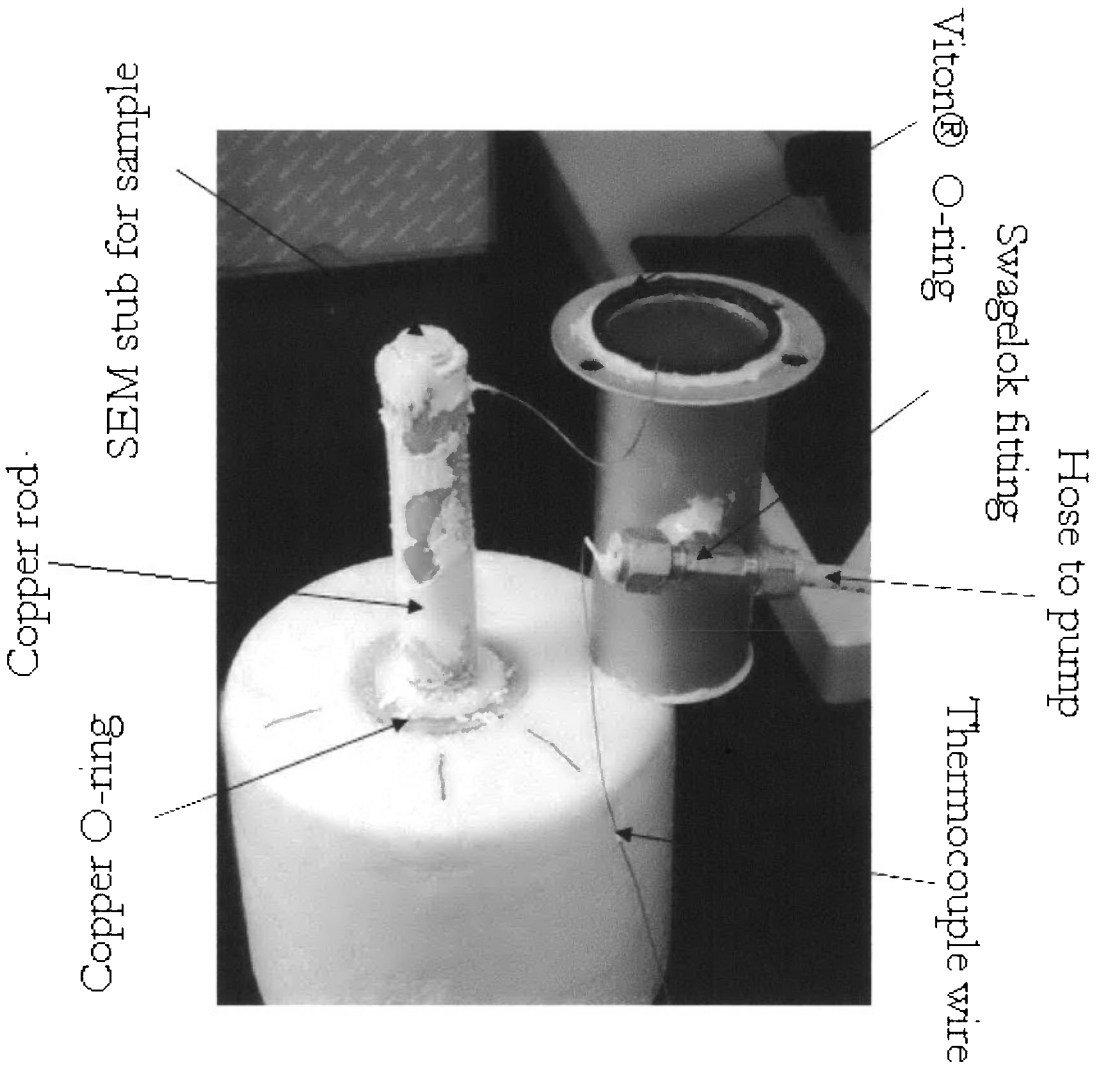

Figure 20. Inner workings of the cryostat.

Discussion

Figure 21 shows our cryostat mounted on the inverted microscope at LLNL. In summary, condensation on the sample surface will interfere with the PL measurement. Figure 20 also shows what happens to the sample if air is allowed in the vacuum tube while the temperature is being reduced. As seen in the photo, frost forms heavily on the sample and the copper rod. This can be reduced by directing a stream of dry nitrogen, or air, onto the copper rod. In the original setup (Figure 15) a stream of dry nitrogen was blown on the sample, but it was not enough to prevent condensation from covering the sample mount. In the revised design (Figure 21), there is a transparent rubber tube provided to blow nitrogen gas onto the base of the cryostat. To further help reduce the vapors from the liquid nitrogen from engulfing the sample, a cover was needed which was introduced in the new set up as seen in Figure 21 in the form of a simple cardboard piece.

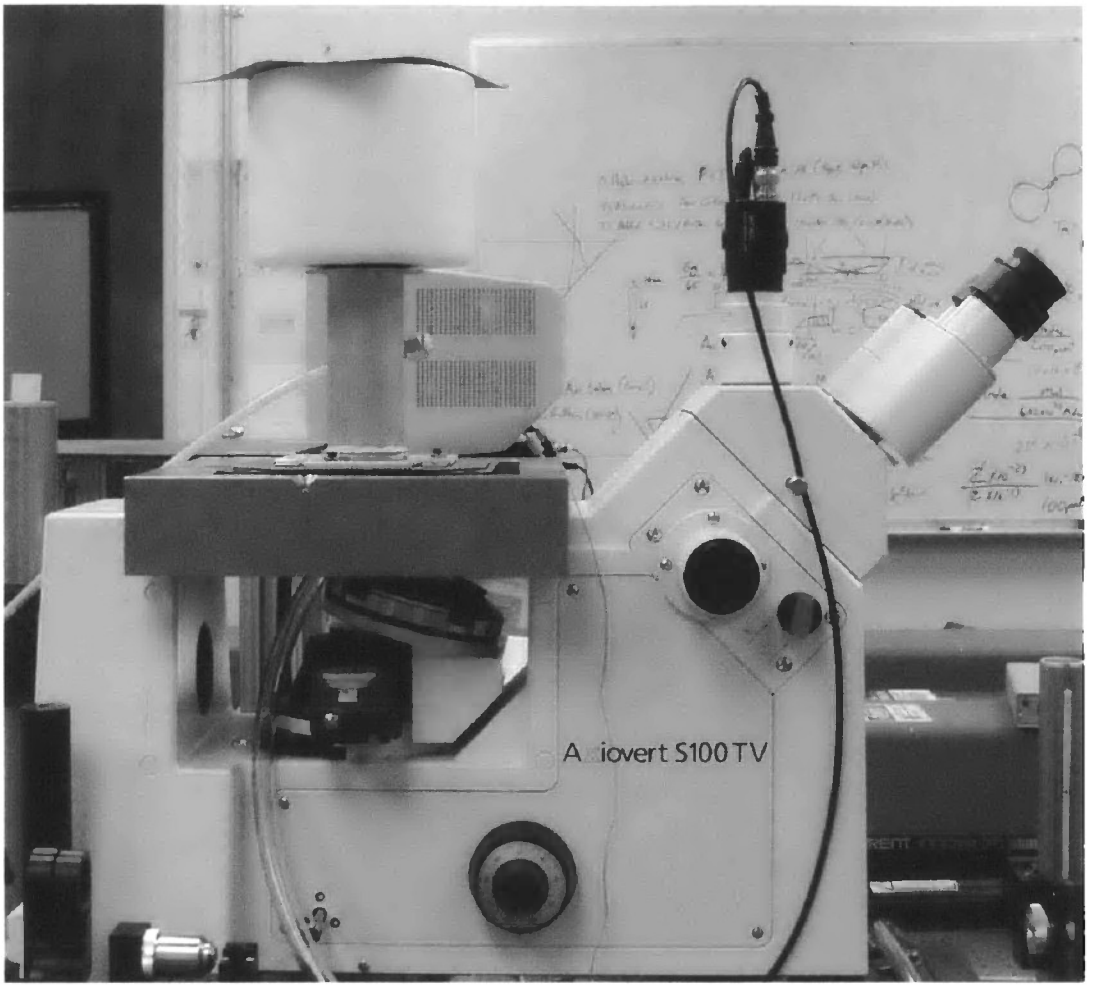

Figure 21. Cryostat mounted on the inverted microscope at LLNL.

Due to the high thermal conductivity of the cooper rod, the mount and sample cooled rapidly to 77K when liquid nitrogen was poured in the Styrofoam 'dewar'. Also, changing the Styrofoam cup in Figure 15 to the dewar in Figure 21 was advantageous in that the extra weight in the new design did in fact add to the dissipation of the bubbling caused by the interaction of the liquid nitrogen and the rod. The length and weight of the copper rod also proved to help solve the vibration problem.

Room Temperature Photoluminescence – CAU

The set up at CAU is on a much smaller scale than that of LLNL. On the excitation side of the setup, a 532 nm laser diode serves as light source. A pair of lenses expands and collimates the laser light. The light is then guided through a Visible/IR beamsplitter, which transmits the visible and rejects near infrared. The ex-citation beam is finally focused to a diffraction-limited 1 micron spot by a 100X microscope objective lens with high numerical aperture (.70). Figure 22 shows a crude drawing of the final plans for this setup.

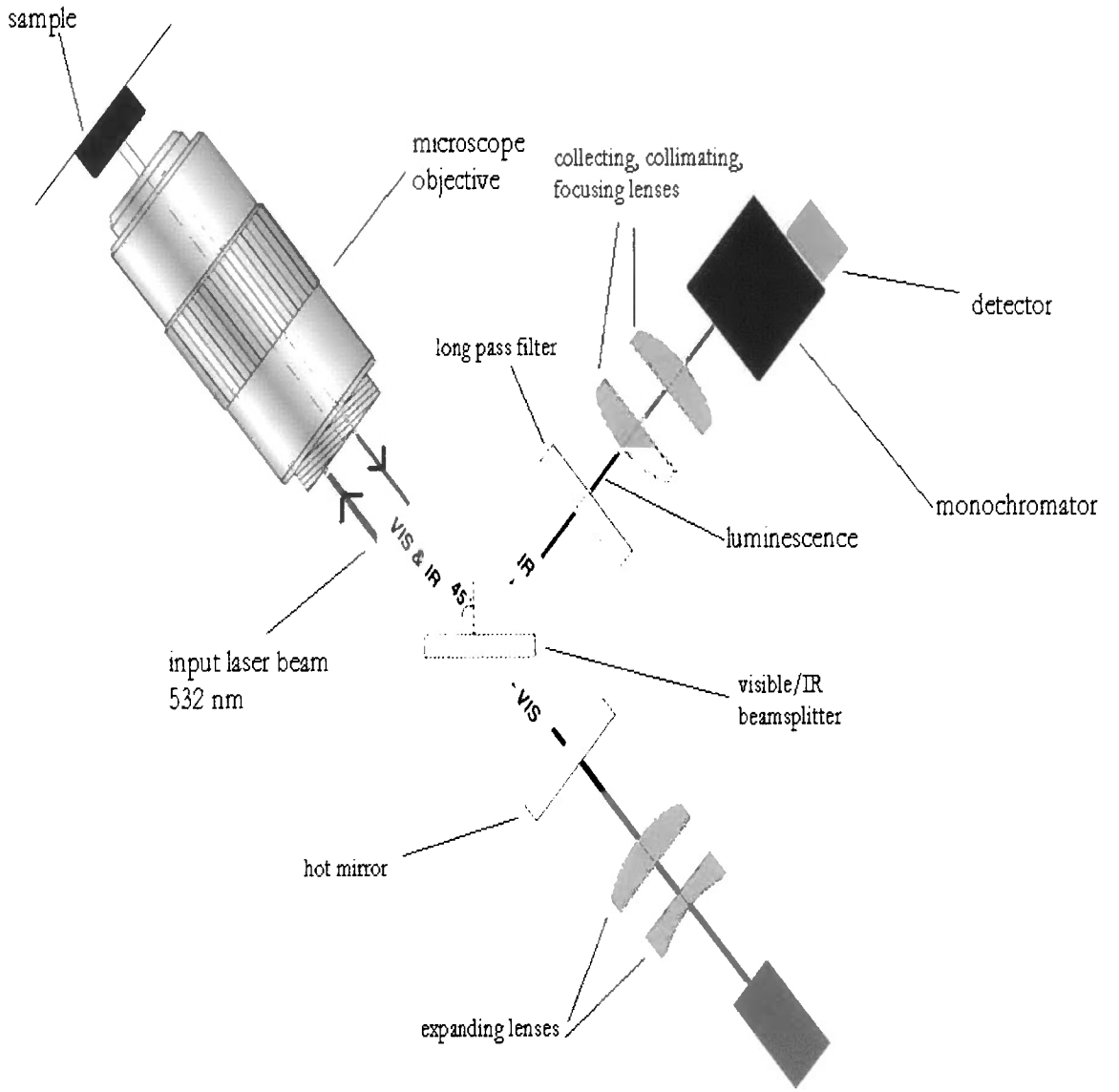

Figure 22. Crude drawing of the final plans for the RT PL spectroscopy setup at CAU (not drawn to scale)

On the detection side, as with the LLNL setup, the locally excited fluorescence is collected by the same microscope objective. The collimated beam passes the Visible/IR beamsplitter where it is then separated in two parts. One arm passes a sharp cutoff (long-pass) filter and is then focused through the entrance slit of an grating monochromator that

disperses the light onto a Si/InGaAs diode housed in a photodetector module. The other arm passes a heat reflecting mirror where the multi-layer dielectric coating on the mirror reflects harmful infrared radiation (heat), while allowing visible light to pass through. It is important to note that Figure 22 is not drawn to scale. Also the excitation and luminescence rays are superimposed and not separated as shown in the drawing.

Components Necessary to Complete Setup

As stated earlier, obtaining the 1 micron spot size was the most important aspect of the optical set up. To find the required spot size, a number of methods were investigated. The elements of exact trigonometric ray tracing become important as the use of lenses play a fundamental role in solving this optical problem. A brief review of the basic properties of lenses will be provided followed by the implementation of these properties to the project at hand.

Elementary ray traces showing the formation of an image using ideal thin lens are shown in the following figures. These figures show an object of height y_1 at a distance s_1 from an ideal thin lens of focal length f. The lens produces an image of height y_2 (or y_3) at a distance s_2 (or s_3) on the far side of the lens. *Ideal thin lens* simply means a lens whose thickness is sufficiently small that it does not contribute to its focal length [28]. In the applications described here, all theoretical assumptions are made working with ideal thin lenses. Consideration of aberrations and thick-lens effects will also not be included.

$$\frac{y_2}{y_1} = \frac{s_2}{s_1} = \frac{f_2}{f_1} = M \tag{2}$$

The quantity M is the magnification of the object by the lens.

$$\frac{1}{f} = \frac{1}{s_1} + \frac{1}{s_2} \tag{3}$$

Eqn? is the *Gaussian lens equation.* This equation provides the fundamental relation between the focal length of the lens and the size of the optical system. [28].

θ is described as the beam divergence (angle). In addition to the assumption of an ideal thin lens, work is also done using the paraxial approximation; i.e. angles are small and we can substitute θ in place of sin θ. Hence:

$$y_2\theta_2 = y_1\theta_1 \tag{4}$$

is a fundamental law of optics. In any optical system comprising only lenses, the product of the image size and ray angle is a constant, or invariant, of the system. This is known as the optical invariant. The result is valid for any number of lenses [28] and is valid in the paraxial approximation.

Although only a brief review of the fundamental laws of optics is provided here, [28] offers more detailed information on these concepts.

Method 1: Focusing the laser beam

The first application chosen to achieve the desired spot size was simply to focus the collimated laser beam to a small spot. This is a common application, and the situation is shown in Figure 23. Here a laser beam, with radius y1 and divergence θ1 is focused by a lens of focal length f.

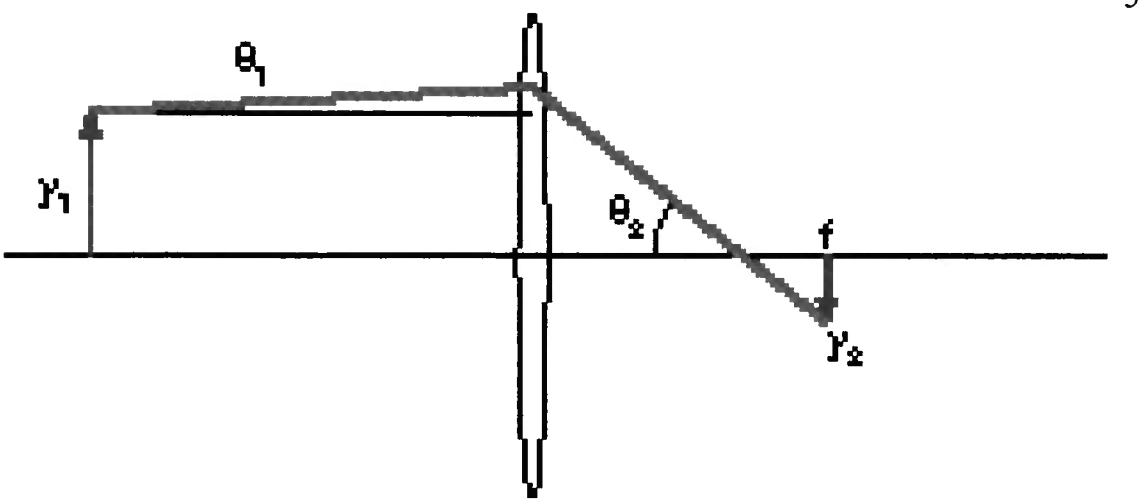

Figure 23. Focusing a collimated beam.

From the figure,

$$\theta_2 = \frac{y_1}{f}$$

From the optical invariant, it is seen that

$$y_2 = \theta_1 f \tag{5}$$

because the product of radius and divergence angle must be constant.

As a numerical example, the 532nm laser diode has a beam diameter of 1.30mm and a divergence of <1.0mrad. These are beam diameter and full divergence, so in the notation of figure?, y_1 = 0.65 mm and θ_1 = 0.5 mrad. Thus, at the focused spot, the radius is $\theta_1 f$. If the diameter of the spot, y_2, is 1μm, then from equation 5, f =2mm. This method simply uses a Plano convex lens to focus the collimated beam to a point. Because of the parameters of the 532nm beam, i.e., the numerical values of the diameter and divergence angle, this beam is considered as being collimated.

The problem arises in the fundamental limitation of the minimum size of the focused spot in this application. It has already been assumed that the lens is a perfect,

aberration-free lens. No improvement of the lens can yield any improvement in the spot size. The only way to make the spot size smaller is to use a lens of shorter focal length or expand the beam. If this is not possible because of a limitation in the geometry of the optical system, then this spot size is the smallest that could be achieved. In addition, diffraction may limit the spot to an even larger size. This basically suggests that even if theoretically a 1 micron spot size is achieved with the chosen lens, the spot could actually be on the order of 2 to 10 times the calculated spot size due to aberrations.

Method 2: Expanding then Focusing the Laser Beam

Expanding the beam: This method involves first expanding a laser beam then incorporating method 1 to focus it down to a small spot. Expanding a laser beam is another commonly used method in optics. Here, at least two lenses are necessary. In Figure 24, a laser beam of radius y_1 and divergence θ_1 is expanded by a negative lens with focal length $-f_1$.

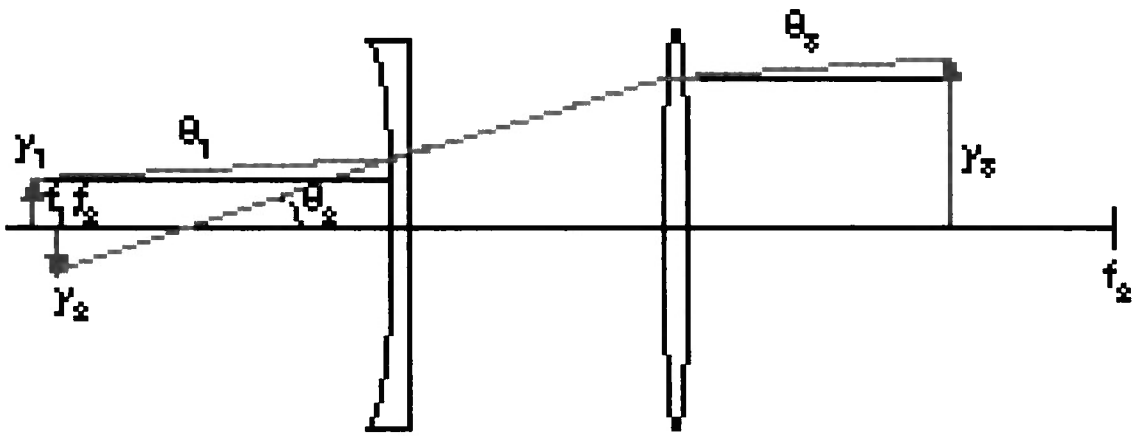

Figure 24. Lens setup to expand and collimate a laser beam

The following equations are obtained from Figure 24:

$$\theta_2 = \frac{y_1}{|-f_1|}$$

and the optical invariant implies that the radius of the virtual image formed by this lens is

$$y_2 = \theta_1 |-f_1| \tag{6}$$

This image is at the focal point of the lens, $s_2 = -f_1$, because a well-collimated laser yields $s_1 \sim \infty$, so from the Gaussian lens equation $s_2 = f$. Adding a second lens with a positive focal length f_2 and separating the two lenses by the sum of the two focal lengths $-f_1 + f_2$, results in a beam with a radius

$$y_3 = \theta_2 |-f_2| \tag{7}$$

and divergence angle

$$\theta_3 = \frac{y_2}{f_2}$$

The expansion ratio or the ratio of the focal lengths of the lenses is

$$\frac{y_3}{y_1} = \frac{\theta_2 f_2}{\theta_2 |-f_1|} = \frac{f_2}{|-f_1|} \tag{8}$$

The expanded beam diameter is

$$2y_3 = 2\theta_2 f_2 = 2y_1 \frac{f_2}{|-f_1|} \tag{9}$$

The divergence angle of the resulting expanded beam

$$\theta_3 = \frac{y_2}{f_2} = \theta_1 \frac{|-f_1|}{f_2} \tag{10}$$

is reduced from the original divergence by a factor that is equal to the ratio of the focal lengths $|-f_1|/f_2$. For instance, to expand a laser beam by a factor of five could be done with a selection of two lenses whose focal lengths differ by a factor of five. The divergence angle of the expanded beam would then be 1/5th the original divergence angle [28].

Focusing the beam: Figure 25 (not drawn to scale) represents a combination of both methods. The planoconcave lens (L1) expands the beam, L2, the first planoconvex lens then collects and collimates the light. Planoconvex lens L3 is finally used to focus this expanded beam to a point. There were many steps taken to achieve the final method used to get the desired spot size.

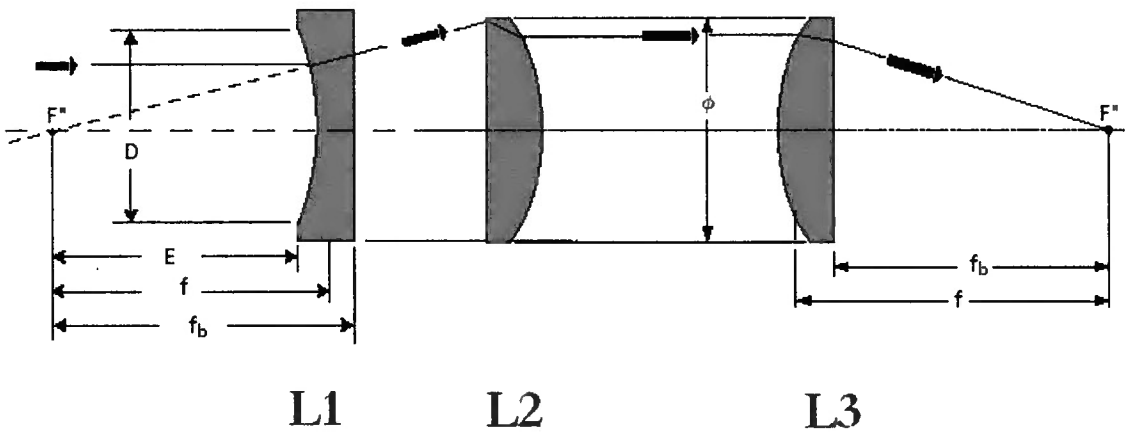

Figure 25. Lens combination of methods 1 and 2. L1 – expanding the beam, L2 – collimating the beam, L3 – focusing the beam to required spot size

Table 4 uses the above diagram to calculate the diameter of the expanded beam (2Y3) and its divergence (θ3). It also shows the focal lengths needed for various magnifications, all in effort to achieve a 0.9μm spot size. As seen in Table 4, the first

problem faced with this setup is that for L3 a lens with a focal length smaller than the diameter of the lens is needed. A planoconvex lens can have a diameter approximately equal to the effective focal length but not be larger. This is an example of a "limitation in the geometry" mentioned earlier.

As a solution, there exists a thin lens equation for lenses in contact. For L3 with focal length f_3, interchanging it with two lenses A and B gives:

$$\frac{1}{f_3} = \frac{1}{f_a} + \frac{1}{f_b} \tag{11}$$

As a numerical example, Table 5 shows an example of theoretically focusing the laser diode beam down to 0.9 microns using a 10X magnification (**M**). For instance, after going through the expansion lens, the beam diameter (**2Y3**) would be 13mm. The focusing lens combination would consist of two lens with focal lengths that satisfy the above equation such that F3 would be greater than 13mm. With that, as seen from the table, this can be achieved from the lenses of focal lengths, fa =25.4mm and fb = 50.8mm. The focal lengths in the table were chosen based on commercial availability from a number of optics vendors.

Table 4. Calculation of the diameter, divergence of the expanded beam, and focal lengths necessary to obtain 0.9μm spot

Y1	θ1	Y3	2Y3	θ3	Y4	θ4	Abs(F1)	M	F2	F3
Radius of laser (mm)	divergence angle of laser (mrad)	Radius of expanded beam (mm)	Diameter of beam	divergence of expanded beam (mrad)	radius of spot (microns)	divergence of spot (mrad)	focal length of 1st lens (mm)		focal length of 2nd lens (mm)	Focal length of 3rd lens (mm)
0.65	0.5	3.25	6.5	0.1	0.45	0.72	10	5	50	4.5
0.65	0.5	6.5	13	0.05	0.45	0.72	10	10	100	9
0.65	0.5	9.75	19.5	0.033333	0.45	0.72	10	15	150	13.5
0.65	0.5	13	26	0.025	0.45	0.72	10	20	200	18

Table 5. Calculation of the diameter, divergence of the expanded beam, and focal lengths necessary to obtain 0.9μm spot using equation 11 for lenses in contact

Y1	θ1	Y3	2Y3	θ3	Y4	θ4	F1	M	F2	Fa	Fb	F3
radius of laser (mm)	Divergence angle of laser (mrad)	radius of expanded beam (mm)	Diameter of expanded beam	divergence of expanded beam (mrad)	radius of spot (microns)	divergence of spot (mrad)	focal length of 1st lens (mm)		focal length of 2nd lens (mm)	Focal length of lens A	Focal length of lens B	focal length of 3rd lens (mm)
0.65	0.5	6.5	13.0	0.05	0.45	1.54	10	10	100	6.35	12.7	4.23
0.65	0.5	6.5	13.0	0.05	0.45	0.77	10	10	100	12.7	25.4	8.47
0.65	0.5	6.5	13.0	0.05	0.45	0.64	15	10	150	12.7	50.8	10.16
0.65	0.5	6.5	13.0	0.05	0.45	0.38	15	10	150	25.4	50.8	16.93

Even with the lenses in contact and the thin lens equation a new problem arose in that the spherical aberrations quickly added up. To reduce these aberrations an achromat can be substituted for the planoconvex "lens b". Figure 26 shows the difference in spherical aberrations obtained by both planovex lenses and achromats.

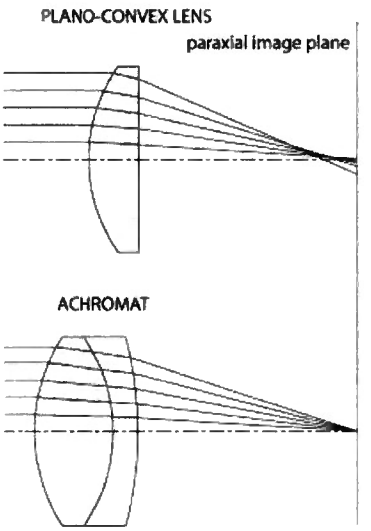

Figure 26. Difference in spherical aberrations for planoconvex lenses and achromats.

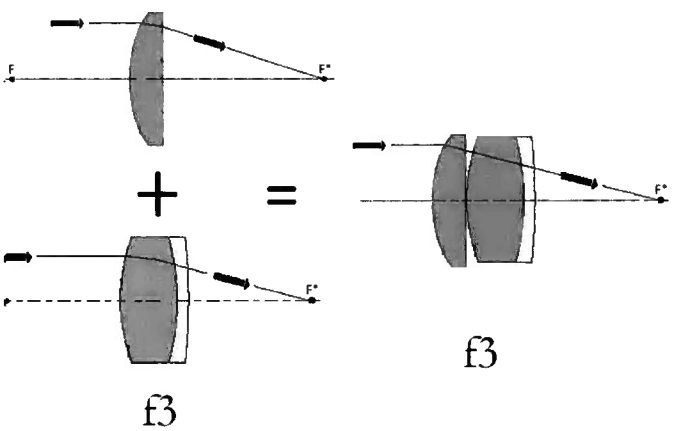

Figure 27. Lens combination of F3 for lenses in contact

Theoretically, a 1 micron spot size is achievable with this set up. However, after further consideration, implementing this experimentally would not give a very tight spot. This would mean different regions of the sample would be probed at different levels in excitation resulting in unreliable data. At LLNL, they achieved this spot size by using microscope objectives to focus the expanded beam to a point. L3 was therefore replaced by a microscope objective as seen in Figure 28.

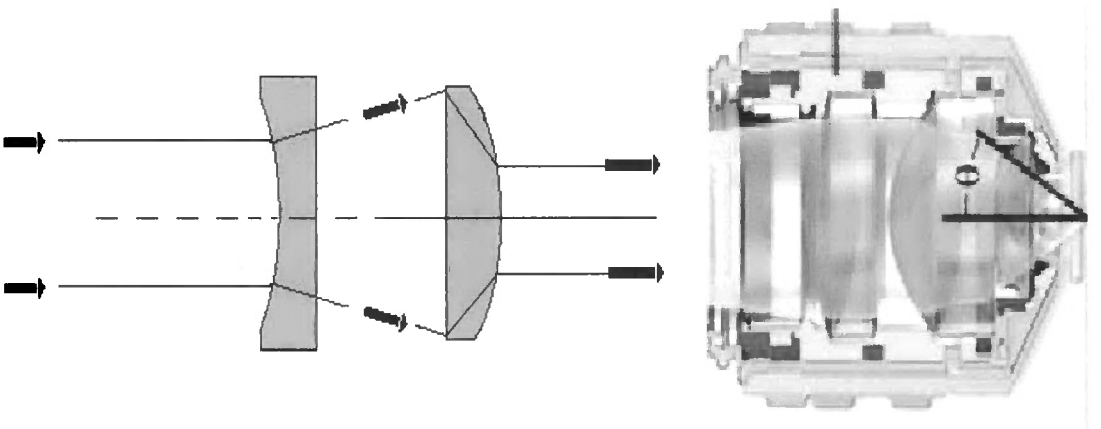

Figure 28. Substitution of lenses in contact with microscope objective. Final design investigated to get a tight 1 micron laser spot size

A simple equation relating the minimum attainable spot size to the wavelength λ, and the f-number *f*/# :

$$\text{spot diameter} = \frac{4\lambda}{\pi} f/\# \tag{12}$$

and for small ϕ

$$\text{f/\#} = \frac{\text{f}}{\text{D}} \approx \frac{1}{2NA} \tag{13}$$

$$\therefore \text{ spot diameter } \simeq \frac{2\lambda}{\pi NA} \tag{14}$$

Substituting the known parameters for this project gives a spot size of

$$\frac{2(532nm)}{\pi(0.70)} = 483.83nm = 0.483\mu m$$

Discussion

Usually, the smallest spot size is desired on target in focusing applications, but there is a limit to how small or tightly the beam can be focused. To get the smallest diameter beam, a very fast lens (one with short focal distance) must be used, but it turns out that lens aberrations become much more pronounced as the focal length gets shorter. In replacing lenses in contact with a microscope objective equation 14 is used as an approximation for minimum achievable spot size. It should be noted that f# is impractical when less than unity, so in general the smallest achievable spot size on target is equivalent to the wavelength of the light used. In principle, this is why smaller spot sizes can be achieved with UV YAG lasers than with CO_2 lasers.

The setup described above cannot be used for LT data collection due to the orientation of the sample and the laser – unless a commercial cryostat is available for use. On the other hand, the setup at LLNL can be used for both RT and LT data readings.

For optimum results, there are a number of things to take into consideration. For minimal aberrations, it is best to use a plano-concave lens for the negative lens and a plano-convex lens for the positive lens with the plano surfaces facing each other. To further reduce aberrations, only the central portion of the lens should be illuminated, so choosing oversized lenses is often a good idea. This style of beam expander is called

Galilean (see Figure 29). Two positive lenses can also be used in a Keplerian beam expander design (also Figure 29), but this configuration is longer than the Galilean design and does not suit the size restraint on CAU's optical system.

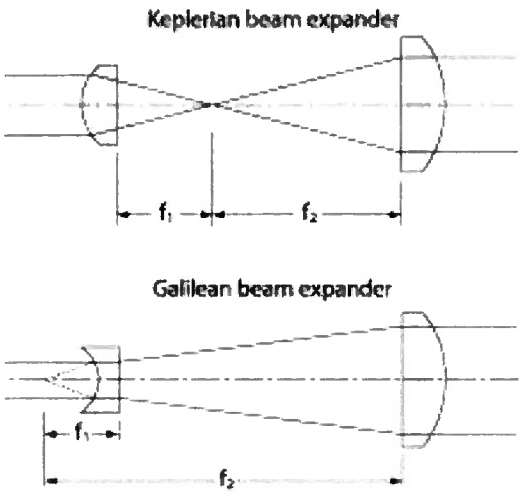

Figure 29. Types of beam expanders – Galilean beam expander used in this project mainly because of space restrictions

Data & Results

At LLNL both RT and LT data for the sample was obtained. However, due to problems in the design, there is deliberation on whether or not the data are useful. In the preliminary stages, Figures 30a and 30b respectively show RT and LT images of the same well with temperature being the only differing factor in the setup. From these images it is clear that the RT image is blurred and not as sharp or luminescent as the LT image.

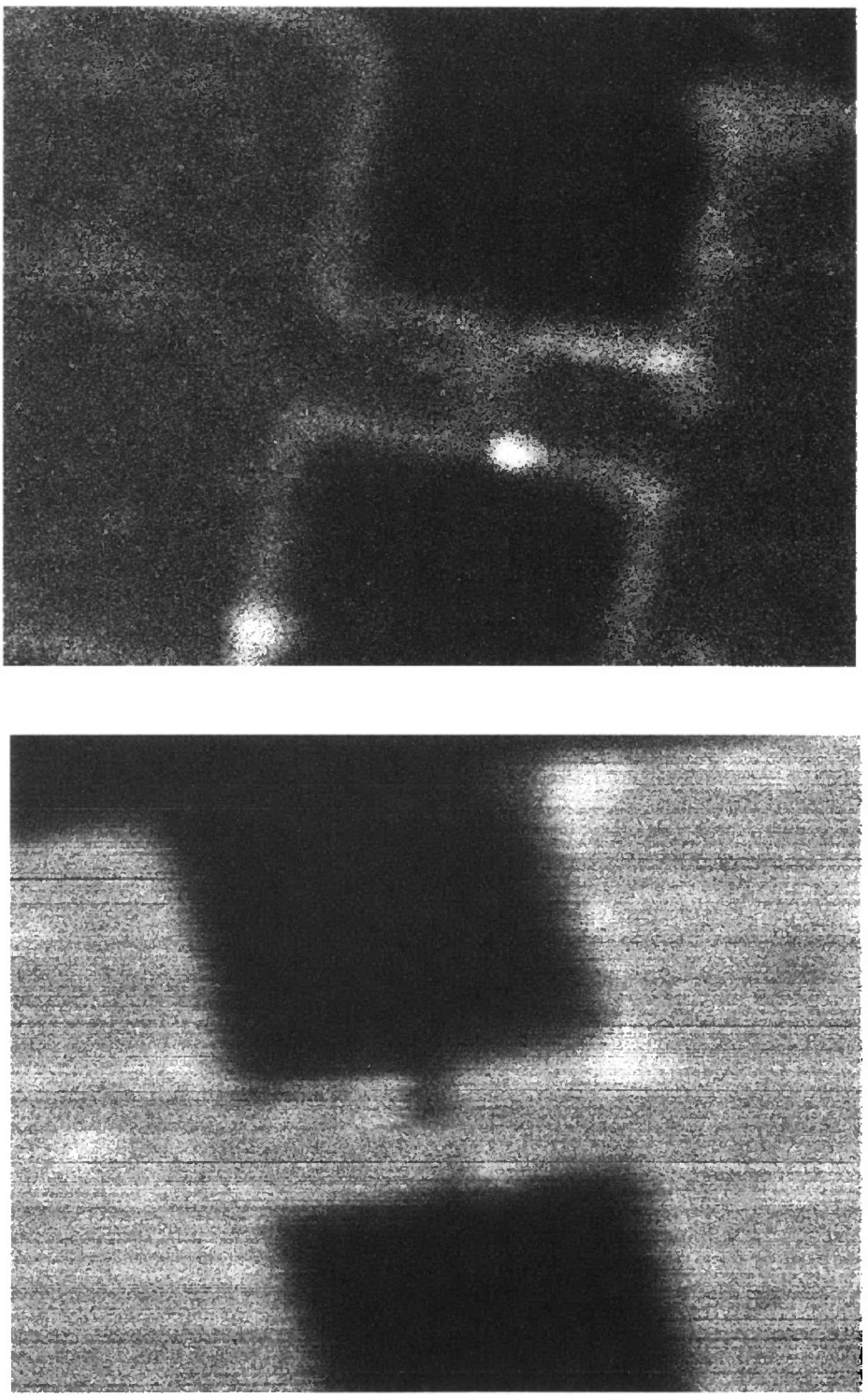

Figure 30. (a) *top* RT image of the QW (b) *bottom* LT image of the same QW.

PL spectra obtained in the initial testing attempts are shown in Figures 31 and 32. The SMPL technique was able to successfully image a FSQW structure consisting of GaAs wells at RT with 632 and 514nm probe beams. Unlike the previous near-field optical microscopy study, both the GaAs quantum well and its supporting posts show a strong contrast in luminescence efficiency with respect to the surrounding GaAs substrate. This is clearly seen in Figure 32, at RT the "pad" and "bridge" both show large peaks in the spectrum below 750nm and smaller peaks around 820nm. At LT the bridge and pad continue to show peaks just around 820nm but nearly all the features seen at RT vanish. Unfortunately, during the process, the system read temperatures below that of liquid nitrogen and condensation formed heavily on the sample. Because of this the results obtained are debatable.

In the first experiment, using just the Styrofoam cup and SEM stub, lifetime measurements were also attempted at room temperature but no emission was detected. This was again attributed to either non-radiative recombination, due to the significant density of surface states (high surface to volume ratio), or inadequate optical absorption length for photoluminescence.

Presently, due to the incomplete design there are no data for room temperature measurements at CAU. However, great progress continues to be made with anticipation of its completion in the near future

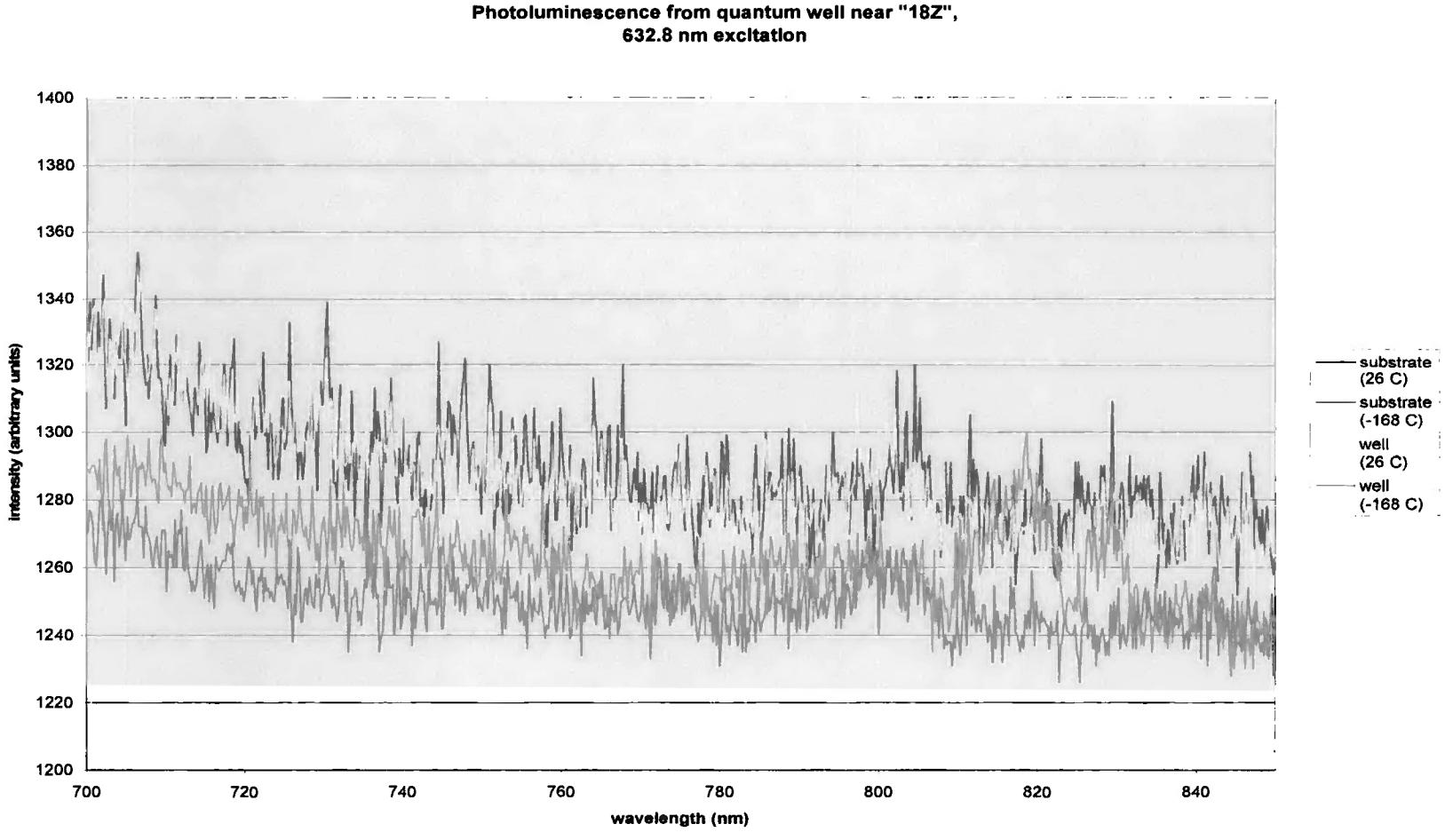

Figure 31. Preliminary data obtained at LLNL with the 632.8 nm laser

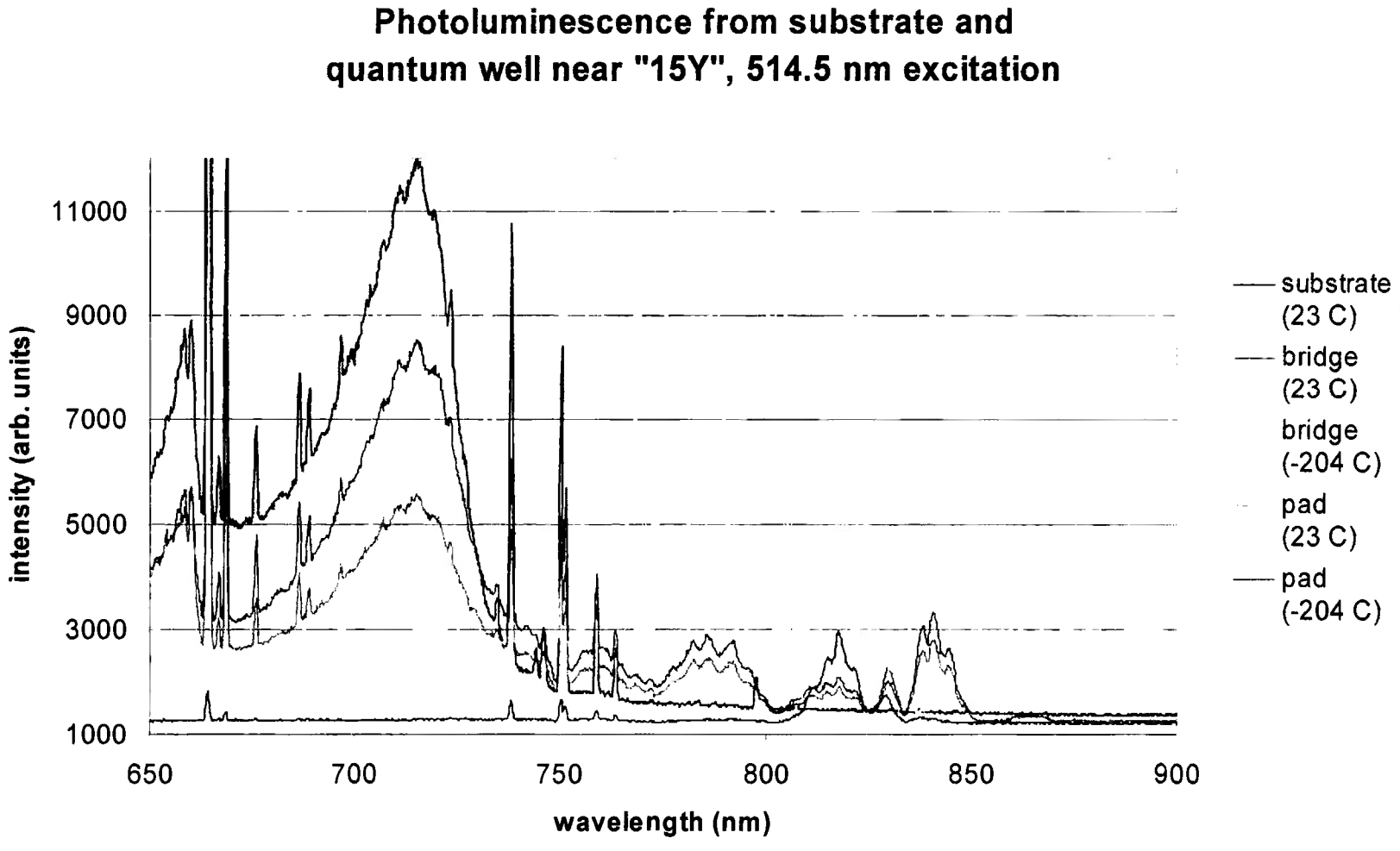

Figure 32. Preliminary data obtained at LLNL with the 514 nm laser

Summary

To recap, it has been stated that surfaces of metals have impurities and defects, and that since PL is nondestructive, it can detect these defects. Also discussed was the wide use of semiconductors in the construction of optoelectronic devices. Being a surface characterization technique, PL can be used to check impurities and defects in semiconductors thereby helping to produce better quality semiconductors. Literature on the subject suggests that the effect of the defects can be eliminated by reducing the sample temperature below their associated activation energies. As such, this was a developmental project involving the design, development and testing of a hand-made low-cost low-temperature cryostat to take samples down to near liquid nitrogen temperature where new information would be obtained about the sample.

Future Work

This is an ongoing project with many different potential aspects to be investigated. For instance, because the performance of many optoelectronic devices is limited by interface recombination, interface passivation has been studied extensively. Furthermore, the surface state density can be varied with chemical passivation techniques. Hence, the next part of this research would be to develop passivation procedures for controlling surface defect density. The variation of the surface state density is done after the formation of the FSQWs. Passivation techniques include epitaxial growth of lattice-matched semiconductor alloys and a variety of chemical surface treatments. Qualitative evaluation of these techniques is straightforward: an increase in the PL signal indicates a decrease in nonradiative interface recombination.

REFERENCE LIST

1. T.H. Gfroerer, Photoluminescence in Analysis of Surfaces and Interfaces, Encyclopedia of Analytical Chemistry edited by R.A. Meyers (Wiley, Chichester, 2000), pp. 9209-9231.
2. M.F Bailon, E.S. Estacio, A. Somintac, and A.A. Salvador, Low Temperature Photoluminescence of GaAs-epitaxial layers (Nat. Inst. Phys, Philippines, 2001), pp. 1-4.
3. M.D. Ferreira and E.A. Imhoff, "Power Dependent Photoluminescence Spectral Shift in InGaAsP Semiconductors". AMP J. Technol. **2**, 70 (1992).
4. R. Kaminski, Spectroscopy. **2**, 55 (2003)
5. R.A. Riebau "Photoluminescence Spectroscopy of Strained InGaAs/GaAs Structures". Thesis Submitted to Faculty of the Graduate School of the University of Maryland (2002).
6. M. L. Hammond, "Moore's Law: The First 70 years". Semicond. Int. 52 (2004).
7. E.-H. Lee, K. Park, "Potential Applications of Nanoscale Semiconductor Quantum Devices for Information and Telecommunications Technologies". Mater. Sci. & Eng. B, **74**, 1 (2000).
8. F. Rosei, "Nanostructured Surfaces: Challenges and Frontiers in Nanotechnology". J. Phys: Condensed Matt.**16**, S1373 (2004).
9. P. Bhattacharya, Semiconductor Optoelectronic Devices, (Prentice Hall, New Jersey, 1996), pp. 10-600.
10. S. Kayali, *GaAs MMIC Reliability Assurance Guideline for Space Applications: GaAs Material Properties* (JPL Publication, California, 1996), pp. 16-23.

11. J.M. Karam, B. Courtois, M. Holio, J.L. Leclercq, P. Viktorovitch. Proceed. SPIE. **2879**, 315 (1996).

12. G. Gibbons, "Gallium Arsenide Electronics". Phys. Technol. **18**, 5 (1987).

13. J.-B. Xia, K. Chang, S.-S. Li, "Electronic Structure and Optical Property of Semiconductor Nanocrystallites". Comp. Mater. Sci. **30**, 274 (2004).

14. H. Lüth, "Semiconductor Nanostructures: A New Impact on Electronics". Appl. Surf. Sci. **130**-132, 855 (1998).

15. M.D. Williams, S.C. Shunk, M.G. Young, D.P. Doctor, D. M Tennant, B.I. Miller, "Fabrication of Free-Standing Quantum Wells". Appl. Phys. Lett., **61**, 1354 (1992).

16. R. Bade, A.J. Spring Thorpe, E.H. Sargent, accepted for publication, "Optical Transmission, Reflection, and Photoluminescence Spectra of Bulk and Heterostructure Compound Semiconductors: Experiments for the Undergraduate Laboratory". Canadian Conference on Engineering Education, Fredricton, N.B, 2001.

17. W. E. Moerner, "A Dozen Years of Single-Molecule Spectroscopy in Physics, Chemistry, and Biophysics". J. Phys. Chem. B, **106**, 910 (2002).

18. W. Trabesinger, A. Renn, B. Hecht, U. P. Wild, A. Montali, P. Smith, C. Weder, "Single-Molecule Imaging Revealing The Deformation-Induced Formation of a Molecular Polymer Blend". J. Phys. Chem. B, **104**, 5221 (2000).

19. W. Trabesinger, A. Renn, B. Hecht, U. P. Wild, A. Montali, P. Smith, C. Weder, "Molecular Rearrangments Observed by Single-Molecule Microscopy". Synthetic Metals. **124**, 113 (2001).

20. F. D. Sala, M.F. Raganato, M. Anni, R. Cingolani, M. Weimer, A. Görling, L. Favaretto, G. Barbarella, G. Gigli, "Optical Properties of Functionalized Thiophenes: a Theoretical and Experimental Study". Synthetic Metals. **139**, 897 (2003).

21. C.W. Hollars, S.M. Lane, T. Huser, "Controlled Non-Classical Photon Emission from Single Conjugated Polymer Molecules". Chem. Phys. Lett. **370,** 393 (2003).

22. T. Huser, M. Yan, "Solvent-Related Conformational Changes and Aggregation of Conjugated Polymers Studied by Single Molecule Fluorescence Spectroscopy". J. Photochem. Photobio. A, **144**, 43 (2001).

23. V.V. Krivolapchuk, M.M. Mezdrogina, N.K. Poletaev, "Effect of Correlation between the Shallow and Deep Metastable Level Subsystems on the Excitonic Photoluminescence Spectra in n-GaAs". Phys. Solid State **45**, 28 (2003).

24. C. Hilsum, A.C. Rose-Innes, Semiconducting III-V Compounds (Macmillan Co., New York, 1961) pp. 27-86

25. O. Madelung, Physics of III-V Compounds, translated by D. Meyerhofer (Wiley & Sons, New York, 1964) pp. 349-369.

26. J. C. Bourgoin, H.J von Bardeleben, D. Stievenard, "Native defects in gallium arsenide", J. Appl. Phys. **64**, 65 (1988).

27. Bart Van Zeghbroeck, Principles of Semiconductor Devices, (Colarado University, 2004).

28. Newport Catalog, *Focusing and Collimating*: Optics and Mechanics (1999/2000) pp. 11-2 – 11-5.

Additional/ Related References

- P. Perlin, W. Trzeciakowski, E. L. Staszewska, J. Muszalski, "The Effect of Pressure on the Luminescence from Gaas/Algaas Quantum Wells" Semicond. Sci. Technol. **9,** 2239 (1994).
- H. Wang, J. Shah, T.C. Damen, "Spontaneous Emission of Excitons in GaAs Quantum Wells: Role of Momentum Scattering". Phys. Rev. Lett. **74**, 3065 (1995).
- D.S. Jiang, H. Jung, K. Ploog, "Temperature Dependence of Photoluminescence from GaAs Single and Multiple Quantum Well Heterostructures Grown by Molecular Beam Epitaxy". J. Appl. Phys. **64,** 1377 (1988).
- K. Kobayashi, T. Ota, K. Maehashi, H. Nakashima, Y. Ishiwata, S. Shin "Photoluminescence inner core excitation in semiconductor quantum structures". Physica. E, 7, 595 (2000).
- M. Gallart, S. Varoutsis, J. Bylander, E. Moreau, I.R. Philip, I. Abram, J. M. Gerard, "Single photon emission from individual semiconductor Nanostructures". Physica. E , **17**, 568 (2003).
- S. Moehl, Hui Zhao,a) B. Dal Don, S. Wachter, and H. Kalt, "Solid Immersion Lens-Enhanced Nano-Photoluminescence: Principle and Applications". J. Appl. Phys. **93**, (2003).
- Gordon E. Moore, "Cramming More Components onto Integrated Circuits". Electronics. **38**, (1965).

- T. Huser, M. Yan, "Aggregation quenching in thin films of MEH-PPV studied by near-field scanning optical microscopy and spectroscopy". Synthetic Metals. **116,** 33 (2001).
- N. Bannov, V. Aristov and V. Mitin, "Temperature Dependence of Electron Mobility in a Free - Standing Quantum Well". Solid State Comm. **93**, 483 (1995).
- X. Sunney Xie, Jay K. Trautman, "Optical Studies of Single Molecules at Room Temperature". Annual Rev. Phys. Chem. **49,** 441 (1998).
- Deepak, and N. Lakshminarayana, "A Detailed Model for Defect Concentration and Dopant Activation in GaAs" .Bull. Mater. Sci. **24**, 225 (2001).
- M. Stellmacher, R. Bisaro, P. Galtier, J. Nagle, K. Khirouni, J.C. Bourgoin, "Defects and Defect Behaviour in GaAs Grown at Low Temperature". Semicond. Sci. Technol. **16**, 440 (2001)
- M.C. Roco, "Broader Societal Issues of Nanotechnology". J. Nanoparticle Res. **5**, 181 (2003).
- R. E. Palmer, "New Directions in Nanoscience: New Challenges for Surface Analysis". Surf. Interface Anal. **34**, 3 (2002).
- M. F.Hochella Jr., "Nanoscience and Technology: The Next Revolution In The Earth Sciences". Earth and Planetary Sci. Lett. **203** 593 (2002).